

B. TECH. PROJECT REPORT

On

Synthesis and Characterization of High Entropy Alloys for Advanced Nuclear Reactors

BY

PATIL CHETAN EKNATH

160005023



**DISCIPLINE OF METALLURGY ENGINEERING AND
MATERIALS SCIENCE
INDIAN INSTITUTE OF TECHNOLOGY INDORE**

December 2019

**SYNTHESIS AND CHARACTERIZATION OF HIGH ENTROPY ALLOYS FOR
ADVANCED NUCLEAR REACTORS**

A PROJECT REPORT

*Submitted in partial fulfillment of the
requirements for the award of the degrees*

of

BACHELOR OF TECHNOLOGY

in

METALLURGY ENGINEERING AND MATERIALS SCIENCE

Submitted by

Patil Chetan Eknath

160005023

Guided by

Dr Sumanta Samal

Assistant Professor, MEMS Department, IIT Indore

Dr Poulami Chakraborty

Scientific Officer -E, Materials Science Division, BARC, Mumbai



INDIAN INSTITUTE OF TECHNOLOGY INDORE

December 2019

CANDIDATE'S DECLARATION

We hereby declare that the project entitled “**Synthesis and Characterization of High Entropy Alloys for Advanced Nuclear Reactors**” submitted in partial fulfillment for the award of the degree of Bachelor of Technology in ‘Metallurgy Engineering and Materials Science’ completed under the supervision of **Dr. Poulami Chakraborty SO/E Materials Science Division and Dr. Sumanta Samal, Assistance Professor, Metallurgy Engineering and Material Science** IIT Indore is an authentic work.

Further, I declare that I have not submitted this work for the award of any other degree elsewhere.

Patil 20-11-2019

Patil Chetan Eknath

CERTIFICATE by BTP Guides

It is certified that the above statement made by the student is correct to the best of our knowledge.

Poulami Chakraborty
Dr. Poulami Chakraborty 20/11/2019

Scientific Officer -E

Materials Science Division

BARC, Mumbai

Poulami Chakraborty Srivastava
Scientific Officer
Bhabha Atomic Research Centre
Trombay, Mumbai- 400085

S. Samal
29/11/2019

Dr Sumanta Samal

Assistant Professor

MEMS Department

IIT Indore

Dr. Sumanta Samal
Assistant Professor
Discipline of MEMS
Indian Institute of Technology Indore
Simrol, Khandwa Road, Indore 453 552

PREFACE

This report on “Synthesis and Characterization of High Entropy Alloys for Advanced Nuclear Reactors” is prepared under the guidance of Dr. Sumanta Samal, Assistant Professor, MEMS Department, IIT Indore and Dr. Poulami Chakraborty Scientific Officer-E, Materials Science Division, BARC, Mumbai.

During this project, I was involved in the development of various High Entropy Alloys (HEAs) for fission and fusion based advanced nuclear reactors. I had carried out various theoretical calculations and simulations to predict the final microstructure of the targeted HEAs. I had prepared two new equiatomic high entropy alloys, namely AlZrNbTiV and WCrMnV for fission and fusion based nuclear reactor applications, respectively. In this project work, we mainly synthesized the HEAs through the melting or powder route and then followed by characterization using sophisticated instruments to obtain microstructural information of the alloy.

I have tried to the best of my abilities and knowledge to explain the content in a simple, proper, and visualized manner. For better understanding, I have attached figures, graphs, and tables wherever it is required to explain.

Patil Chetan Eknath

B.Tech. IV Year

Discipline of Metallurgy Engineering and Materials Science

IIT Indore.

ACKNOWLEDGEMENTS

I have devoted my sincere efforts in the process of accomplishment of this project. However, it would not have been possible without the kind support and guidance of Dr. Sumanta Samal and Dr. Poulami Chakraborty. I, therefore, would like to extend my sincere thanks to all of them.

I would to express my deepest sense of gratitude to Dr. Parasharam M. Shirage, Head of Department, Dr. Santosh S Hosmani, DUGC Convener and faculty members of my department specially Dr Vinod Kumar for their valuable time and support.

I am highly indebted to Shri. Ravi Hankare and Shri Suman Bukya for their help in lab work and providing the necessary practical knowledge. I would like to express my gratitude towards Staff members of Materials Group, BARC for their kind co-operation and encouragement which helped me in the completion of this project.

Finally, I would like to express my sincere gratitude to each and every one who had helped me throughout my training period.

Patil Chetan Eknath

B.Tech. IV Year

Discipline of Metallurgy Engineering and Materials Science

IIT Indore.

ABSTRACT

Synthesis and characterization of two equiatomic ZrNbTiVAl and WCrMnV high entropy alloys are done in the present study. Equiatomic novel refractory ZrNbTiVAl high entropy alloy with a low density of 5.76 g cm^{-3} was produced by levitation melting method. Electron microscopic analysis coupled with X-ray diffraction technique has revealed that dendrite region shows ordered body centered cubic (B2) phase while inter-dendritic region shows Zr₅Al₃ and ZrAl₂ type intermetallic phases. It is well known that single BCC phase materials exhibit better resistance to void swelling and low irradiation induced chemical segregation than that of multiphase materials. ZrNbTiVAl high entropy alloy has BCC_B2 with lattice parameter of 0.32628 nm as a major phase and also shows low neutron absorption cross-section (0.0188 b) which makes it a candidate material for advanced fission based nuclear reactors. Heat treatments were done at 950 deg c for 7,15,20 and 25 hours and at 1200 deg c for 24 hours for homogenization. Recrystallized structure was observed in sample which was heat treated at 1200 deg c for 24 hours. Heat treatments revealed that Zr and Al tries to come together at one region (inter-dendritic, grain boundary) while other elements in other region (dendritic, grain). Microhardness of as cast sample is 576.663 HV and it continues to increase as temperature increases with constant time or vice versa due to increase in fraction of second phase particles

CALPHAD study of equiatomic WCrMnV high entropy alloy shows single BCC phase for wide range of temperature from 500 deg to ~ 2000 deg (starting point of melting) which makes it the candidate material for first wall in fusion reactors. With the help of vacuum arc melting unit, we have produced single BCC phase with lattice parameter of 3.09437 Å and unmelted tungsten was also found during SEM-EDS analysis which was reflected in XRD pattern (note that Mn was almost evaporated during melting). Small sample of WCrMnV HEA was synthesized by coupling Vacuum Arc Melting unit with Levitation Melter and nearly equiatomic composition at dendritic region and tungsten-vanadium rich composition at inter-dendritic region was confirmed by SEM-EDS analysis. For comparative study, equiatomic WCrMnV HEA was synthesized by powder route using conventional and spark plasma sintering methods. Ball milled powder shows single BCC phase with some peaks (with low intensities and present at lower angles) of Cr, Mn and V. Conventional and spark plasma sintered samples shows BCC phase along with Mn_{9.54}Cr_{14.46}O₃₂ phase. There was difference in phases present in experimental samples and predicted by CALPHAD method as calculations were done for equilibrium condition.

TABLE OF CONTENTS

Title Page	i
Candidate's Declaration	iii
Certificates by BTP Guides	iii
Preface	iv
Acknowledgement	v
Abstract	vi
Table of Contents	vii
List of Figures	viii
Chapter 1 INTRODUCTION AND LITERATURE SURVEY	1
1.1 Introduction	1
1.2 Literature survey	3
Chapter 2 MATERIAL SELECTION FOR ADVANCE NUCLEAR REACTORS	5
2.1 Empirical methods for single phase HEA	5
2.2 CALPHAD (Calculation of Phase Diagrams) method for single phase HEA	7
2.3 AlZrNbTiV HEA selection for Advanced Fission Nuclear Reactors	8
2.4 WCrMnV HEA selection for Fusion Reactor	8
Chapter 3 EXPERIMENTAL METHODOLOGY	10
3.1 Instruments used in the present study	10
3.2. Experimental procedure	15
Chapter 4 RESULTS AND DISCUSSION	23
4.1 SEM analysis of Binary alloys	23
4.2. Characterization of AlZrNbTiV HEA	24
4.3. Micro-hardness of AlZrNbTiV HEA	32
4.4. Discussion on AlZrNbTiV HEA	33
4.5 Characterization of WCrMnV HEA	34
4.6. Microhardness of conventional sintered WCrMnV HEA	41
4.7. Discussion on WCrMnV HEA	41
Chapter 5 CONCLUSION AND FUTURE SCOPE	43
References	

LIST OF FIGURES

Fig. 1 CALPHAD study of equiatomic WCrVMn HEA by using Thermocal software	9
Fig 2 powder route for alloy synthesis	20
Fig 3 (a), (b), (c), (d) SEM micrograph of binary alloys	23
Fig 4(a), 4(b) Optical images of as cast AlZrNbTiV high entropy alloy	24
Fig 4(c), 4(d) and 4(e) SEM micrograph of the cross section of as cast AlZrNbTiV HEA	25
Fig 5 SEM micrograph of the bottom cross section of as cast AlZrNbTiV HEA	25
Fig 6(a) and 6(b) Optical images for sample heat treated at 950 deg c for 7 hours	26
Fig 7(a),7(b) and 7(c) SEM images of heat-treated samples at 950 deg c for 15,20,25 hours	26
Fig 8 Map spectrum of individual elements of heat-treated AlZrNbTiV HEA sample at 950 deg c for 15 hours	28
Fig 9 SEM micrograph of heat-treated sample at 1200 deg c for 24 hours	29
Fig 10 Map spectrum of individual elements of heat-treated AlZrNbTiV HEA sample at 1200deg c for 24 hours	29
Fig 11, 12 XRD graph of as cast AlZrNbTiV HEA	30
Fig 13(a) and 13(b) SEM micrograph of arc melted WCrMnV	34
Fig 14 (a), (b) and (c) SEM micrograph of levitation melted WCrMnV HEA	36
Fig 15(a) and (b) SEM micrograph of bottom and top part of conventional sintered WCrMnV HEA	37
Fig 16 SEM micrograph of spark plasma sintered WCrMnV HEA	38
Fig 17 (a), (b), (c), (d) XRD graph of WCrMnV HEA produced by various routes	39

1 INTRODUCTION AND LITERATURE SURVEY

1.1 Introduction

All advanced nuclear systems should encompass high temperature structural materials, fast neutron resistant core materials and specific reactor and power conversion technologies. The main requirements for materials used in nuclear reactors are as follows [2]:

- 1) Excellent dimensional stability under unprecedented fluxes of high-energy neutrons along with intense thermomechanical stresses.
- 2) Better mechanical properties like tensile strength, ductility, creep resistance, fracture toughness, resilience etc at high temperature.
- 3) Better compatibility with corrosive environment (reactor coolant, moderator, process fluid)
- 4) Neutron radiation damage resistance. Etc.

Conventional materials used in nuclear reactors shows loss in desirable mechanical properties like creep strength, irradiation embrittlement etc at high temperatures which bounds the efficiency of reactors. It is therefore necessary to explore new alloys outside the paradigms of conventional materials to meet these material requirements [1].

High entropy alloys (HEAs) which are usually composed of at least five or more alloying elements in nearly equiatomic percentage have attracted many researcher's attentions because they have excellent high-temperature strength, high hardness, great thermal stability and self-healing ability under irradiation due to the four core effects [11]:

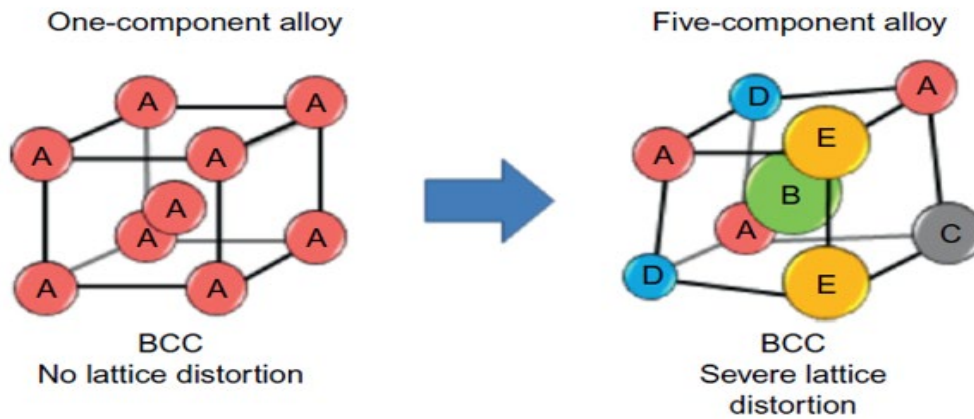
- 1) The high entropy effect:

The configurational entropy change per mole for the formation of a solid solution from n elements with X_i mole fraction is $\Delta S_{\text{conf}} = -R \sum X_i \ln(X_i)$ where R is gas constant. Higher number of elements would potentially lower the mixing free energy, especially at high temperatures by contributing larger configurational entropy

Hence, HEAs have simple phase structure like single BCC/ FCC phase structure or mixture of BCC+FCC phase structure. Solid solution is easier to form in equiatomic high entropy alloys because of maximization in configurational entropy which helps in lowering the Gibbs free energy of solid solution [3].

2) The lattice distortion effect:

Lattice distortion in high entropy alloys arises due to difference in atomic size of elements. Hardness and strength effectively increase because of large solution hardening in the heavily distorted lattice.



Schematic diagram showing large lattice distortion exists in the five-component BCC lattice.

Fig A

3) sluggish diffusion:

It has been proposed that slower diffusion and higher activation energy would occur in HEAs due to larger fluctuation of lattice potential energy (LPE) between lattice sites (Tsai et al., 2013b). The abundant low-LPE sites can serve as traps and hinder the diffusion of atoms. This leads to the sluggish diffusion effect. It also provides various advantages in controlling microstructure and properties: easiness to get supersaturated state and fine precipitates, increased recrystallization temperature, slower grain growth, reduced particle coarsening rate, and increased creep resistance.

4) The 'cocktail' effect:

Cocktail effect is used to emphasize the enhancement of the properties by at least five major elements. HEAs might have single phase, two phases, three phases, or more depending on the composition and processing, the whole properties are from the overall contribution of the constituent phases. This relates with the phase size, shape, distribution, phase boundaries, and properties of each phase. Moreover, each phase is a multicomponent solid solution and can be regarded as an atomic-scale composite. Its composite properties not only come from the basic properties of elements by the mixture rule but also from the mutual interactions among all the elements and from the severe lattice distortion.

Mutual interaction and lattice distortion would bring excess quantities in addition to those predicted by the mixture rule. As a whole, “cocktail effect” ranges from atomic-scale multicomponent composite effect to microscale multiphase composite effect. Cocktail effect was introduced by the interaction of constituent elements in the $Al_xCoCrCuFeAl$ alloy, which leads to a phase transformation from an FCC structure to a BCC when the Al content is increased beyond critical value.

1.2 Literature survey

1.2.1 Conventional materials used in fission-based reactors

Conventional Materials used in nuclear reactors	Application	Limitation
Ferritic/Martensitic steels	Pressure vessel of high temperature gas cooled reactors, Core structure material for fusion reactors	There is significant loss in creep-rupture strength and irradiation embrittlement above 550 deg C
Oxide dispersion strengthened steels	Fuel cladding material for fast neutron reactors	Internal corrosion (oxide clad reaction) and phase transition around 1075 K.
Ceramic materials such as SiC, TiC, ZrC, TiN	Heat exchangers, thermal insulations and core components as control rod sheath and fuel constituents in gas or lead cooled fast reactors	Brittleness
Nickel based alloys (Haynes 230, Inconel 617)	Core material component of Supercritical water reactor.	Inconel 617 suffers from poor corrosion resistance and its high Co content may give rise to potential radioactive contamination problem. Hastelloy XR shows poor creep resistance

1.2.2 High Entropy Alloys (HEAs) for Fusion reactor

Alloy	Composition (atomic %)	Application	Synthesis route
VCrMnTi High Entropy Alloy [21]	(VCrMn) _{100-x} Ti _x Where x=1,2,4,8	In Fusion reactor as a Divertor	Alloys were fabricated as ingots using an arc melting process in an argon atmosphere. The ingots were inverted and re-melted three times to ensure homogeneity. Heat-treatment was done at 1200 deg C for 100 Hours, followed by quenching in water.
WTaCrV High Entropy Alloy [15]	W: 38%, Ta: 36%, Cr: 15% and V: 11%	Candidate for Plasma Facing Wall (PFW) in Fusion reactor	Magnetron Sputtering/E-beam Evaporation Hybrid Physical Vapour Deposition System.
W _x TaTiVCr High Entropy Alloy [15]	WX(TaTiVCr) _{100-X} Where X=0.3,0.4,0.5,0.6, 0.7,0.8,0.9	Candidate for Plasma Facing Wall (PFW) in Fusion reactor	The mixing of elemental W, Ta, Ti, V and Cr powders by planetary ball mill followed by spark plasma sintering at 1600 deg C
VTiFeCrZr High Entropy Alloy [22]	V:35%, Ti:35%, Fe:15%, Cr:10% and Zr:5%	Fusion reactor	vacuum arc melting with high purity elements on a water-cooled copper mould in the argon atmosphere. Ingots were melted at least five times to ensure compositions homogeneous. A sample was cut from the as-cast ingot and annealed at 1000 deg C for 3 h in a vacuum furnace for microstructure comparison.

2 MATERIAL SELECTION FOR ADVANCE NUCLEAR REACTORS

Our main objective is to developed single phase (BCC) high entropy alloy for advanced nuclear reactors. In present study, we have used CALPHAD (calculation of phase diagrams) and empirical methods to develop single phase HEAs for fission and fusion based reactors.

2.1 Empirical methods for single phase HEA [13]

Following parameters decides the formation of single-phase high entropy alloy containing n different elements

1. Atomic size difference (δ):

$$\delta = \sqrt{\sum_{i=1}^n c_i (1 - \frac{r_i}{\bar{r}})^2} \quad \text{where } \bar{r} = \sum_{i=1}^n c_i r_i, \quad c_i \text{ and } r_i \text{ are the atomic percentage and atomic radius of the } i\text{th element.}$$

2. The mixing enthalpy (ΔH_{mix}):

$$\Delta H_{mix} = \sum_{i=1, i \neq j}^n \Omega_{ij} c_i c_j \quad \text{where } \Omega_{ij} = 4 \Delta H_{mix}^{AB}, \quad \Delta H_{mix}^{AB} \text{ is the mixing enthalpy of binary liquid AB alloys which can be calculated using Miedema's model}$$

3. The mixing entropy (ΔS_{mix}):

$$\Delta S_{mix} = -R \sum_{i=1}^n c_i \ln c_i \quad \text{where R is a gas constant}$$

4. Electronegativity difference ($\Delta\chi$):

out of consideration from the classical Hume-Rothery's rule to form solid solution phases. It is defined by

$$\Delta\chi = \sqrt{\sum_{i=1}^n c_i (\chi_i - \bar{\chi})^2} \quad \text{where } \bar{\chi} = \sum_{i=1}^n c_i \chi_i, \quad \chi \text{ is the Pauling electronegativity for the } i\text{th element.}$$

5. Valence Electron Concentration (VEC):

$$VEC = \sum_{i=1}^n c_i (VEC)_i \quad \text{where } (VEC)_i \text{ is the VEC for } i\text{th element.}$$

6. Ω parameter define as

$$\Omega = \frac{T_m \Delta S_{mix}}{|\Delta H_{mix}|} \quad \text{where } T_m \text{ is the melting temperature of alloy calculated by mixture rule}$$

Criteria for formation of single-phase solid solution HEA

- Valence Electron Concentration (VEC) plays a decisive role in determining the fcc- or bcc-type solid solution in HEAs, and especially larger VEC (=8) favours the formation

of fcc-type solid solutions, while smaller VEC (<6.87) favours the formation of bcc-type solid solutions.

- Criterion given by Zhang et al. states that the atomic size differences (δ) should be less than 6.5%, the enthalpy of mixing (ΔH_{mix}) should be in the range of -15 to 5 kJ mol^{-1} and the entropy of mixing (ΔS_{mix}) should be in the range of 12 – 17.5 $\text{J K}^{-1} \text{mol}^{-1}$ for the formation of single phase solid solution.
- Criterion for solid solution phase formation in HEA can be given by $\Omega \geq 1.1$ $\delta \leq 6.6\%$.

Above all seven parameters were calculated for equiatomic AlZrNbTiV and WCrMnV HEA as shown in below tables (table 3 and 4). Equiatomic WCrMnV HEA have satisfied all empirical criteria and hence we can expect single BCC phase for this HEA. Equiatomic AlZrNbTiV HEA have approximately satisfied all empirical criteria (calculated enthalpy of mixing is -17.44 KJ/mol which is more than the value given by Zhang et al. criterion). Hence, there are chances of formation of intermetallic in minor fraction along with solid solution phase

$(\Delta H_{mix})_{ij}$				
j \ i	V	Mn	Cr	
W	-1	6	1	
V		-1	-2	
Mn			2	

Table 1 (enthalpy of mixing of binary ij alloy)

$(\Delta H_{mix})_{ij}$					
j \ i	Zr	Nb	Ti	V	
Al	-44	-18	-30	-16	
Zr		4	0	-4	
Nb			2	-1	
Ti				-2	

Table 2 (enthalpy of mixing of binary ij alloy)

AlZrNbTiV	At %	$r(A^0)$	δr	VEC	X_p	ΔX	ΔH_{mix} (kJ/mol)	ΔS_{mix} (J/K.mol)	$T_m(K)$	Ω
Al	20	1.432	-	3	1.61	-	-	-	933	
Zr	20	1.603	-	5	1.6	-	-	-	2128	
Nb	20	1.429	-	6	2.16	-	-	-	2742	
Ti	20	1.462	-	4	1.54	-	-	-	1943	
V	20	1.316	-	5	1.63	-	-	-	2183	
HEA	100	1.4484	6.34742	4.6	1.708	22.798	-17.44	13.3808	1985.8	1.523

Table 3(Calculated parameters for AlZrNbTiV HEA)

WVCrMn	Atomic %	$r(pm)$	δr	VEC	X_p	ΔX	ΔH_{mix} (kJ/mol)	ΔS_{mix}	$T_m(K)$	Ω
W	25	137	-	6	2.36	-	-	-	3680	
Cr	25	125	-	6	1.66	-	-	-	2130	
Mn	25	135	-	7	1.55	-	-	-	1517	
V	25	132	-	5	1.63	-	-	-	2175	
HEA	100	132.25	3.42144	6	1.8	32.58	1.25	11.52 565	2375. 5	21.903

Table 4 (Calculated parameters for WCrMnV HEA)

2.2 CALPHAD (Calculation of Phase Diagrams) method for single phase HEA [12]

The CALPHAD method, one collects and assesses all available experimental and theoretical information available on phase equilibria and thermochemical properties in a system. The thermodynamic properties of each phase are then described through the Gibbs free energy, applying a mathematical model containing adjustable parameters. These parameters are evaluated by optimizing the fit of the model to all the assessed information, also involving coexisting phases. Following this it is possible to recalculate the phase diagram, as well as the thermodynamic properties of all the phases and the system as a whole. The philosophy of the CALPHAD method is to obtain a consistent description of the phase diagram and the thermodynamic properties so as to reliably predict the set of stable phases and their thermodynamic properties in regions without experimental information and for metastable states during simulations of phase transformations.

2.3 AlZrNbTiV HEA selection for Advanced Fission Nuclear Reactors

In present study, we have selected equiatomic AlZrNbTiV High entropy alloy for structural component in advanced fission nuclear reactors. Elements for this alloy was selected based on following parameters:

1) Low activation elements which is necessary criteria to reduce the amount of high-level radioactive waste upon decommissioning of reactor.

2) Many studies show that materials consisting of single BCC phase shows better irradiation resistance, low void swelling, better compositional homogeneity to irradiation than single FCC phase and multiphase materials, so to get single BCC phase we have selected five elements Nb, Ti, V, Zr and Al because of following reasons:

a) Zr and Ti belong to group IV and Nb and V belong to group V. Therefore, both these sets of elements have complete solubility in each other.

b) Among the five elements, Nb and V exist in bcc structure in their entire solid-state range whereas Zr and Ti have bcc phase in the high temperature region. In addition, alloying of Al in Zr as well as in Ti promotes bcc type phases [9].

c) This combination of elements shows strong tendencies for ordering due to the presence of Al and also shows separation tendencies because of positive interaction parameters between Zr and Nb and between Ti and Nb [10].

Equiatomic HEA of these elements qualify the criteria for single phase HEA given by Zhang et al. which states that the atomic size differences should be less than 6.5%, the enthalpy of mixing should be in the range of -15 to 5 kJ mol⁻¹ and the entropy of mixing should be in the range of $12-17.5$ J K⁻¹ mol⁻¹ [7].

3) Low density of alloy, hence low-density elements i.e. Al and Ti were selected.

2.4 WCrMnV HEA selection for Fusion Reactor

There are main three component namely first wall, blanket, and divertor in fusion reactor as shown in fig.1 which are subjected to high effluence of neutrons carrying 14.1 MeV kinetic energy. The fusion neutrons produce atomic displacement cascades which results in production of point structure defects (vacancies, interstitials) [18] and transmutation nuclear reactions within the materials which yields the formation of impurities (H, He atoms) [6]. Hence there is significant adverse effect on properties like loss of ductility, loss of creep strength, swelling etc.[17]

In present study, we are trying to developed equiatomic WCrMnV high entropy alloy (HEA) for plasma facing wall by choosing reduced activation refractory elements of high

melting point which forms single BCC phase [8]. Empirical criteria confirm the formation of single BCC phase and CALPHAD calculation shows that this HEA contains single BCC_B2 phase for wide range of temperature ranging from 500-degree Celsius to ~ 2000 deg (starting point of melting).

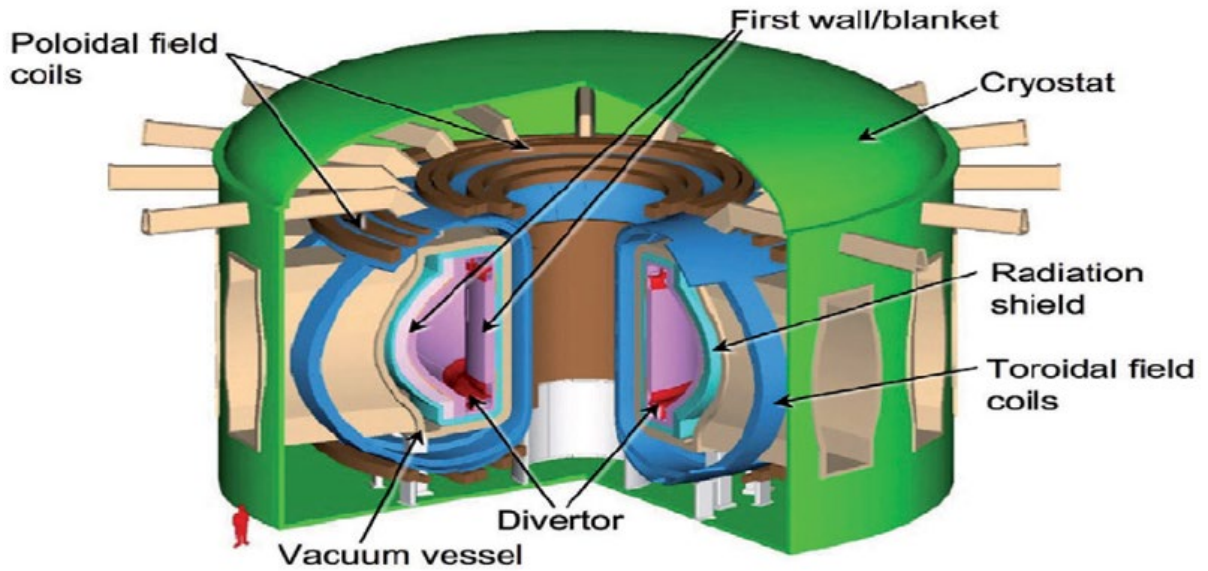


Fig.B, Schematic of key components in a magnetically confined fusion reactor

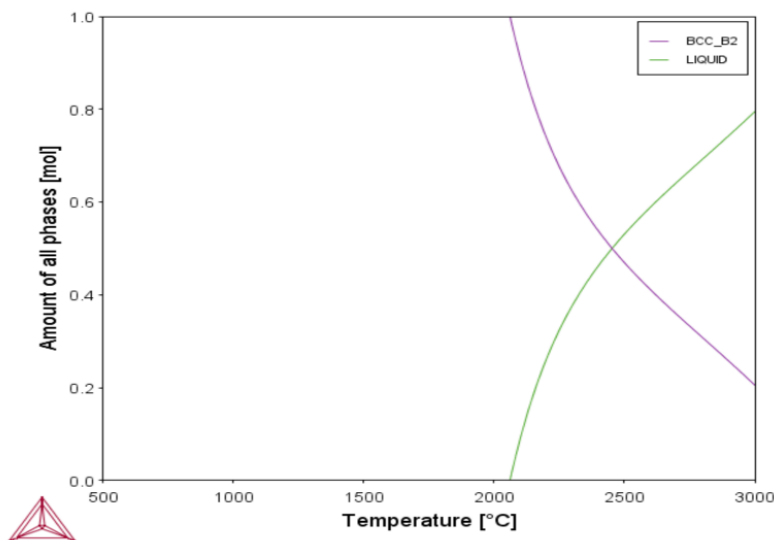


Fig. 1 CALPHAD study of equiatomic WCrVMn HEA by using Thermocal software showing single BCC_B2 phase which is stable from 500 deg C to ~2000 deg C`

3 EXPERIMENTAL METHODOLOGY

3.1. Instruments used in the present study

3.1.1 For melting

1) Vacuum Arc Melting (VAM) unit

In VAM unit, metals undergo melting with an electric arc produced between tungsten electrode and sample in inert atmosphere or vacuum (to avoid oxidation and other contamination) with water-cooled copper crucible. This process is essential for refractory metals such as zirconium, titanium, vanadium and their alloys, as these materials are very reactive. Materials with melting points of up to 2,200°C can be easily melted in vacuum arc furnace. After elemental metals (or master alloy) are melted and solidified, it can be 'turned over' by a 'tweezer mechanism' without breaking the vacuum (and then re-melted).

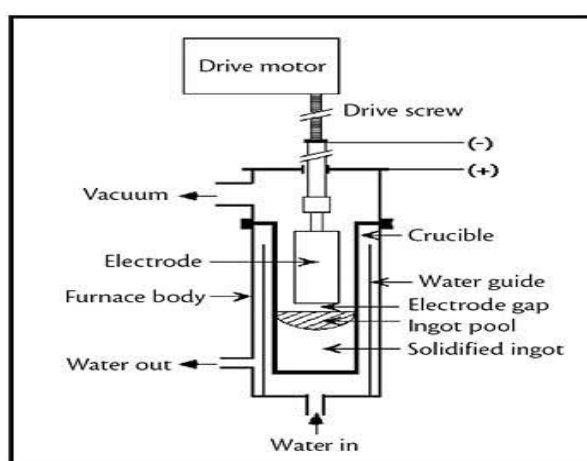


Fig C, Schematics of Vacuum Arc Melting unit

Different part in VAM unit

a) Tungsten Inert Gas (TIG-400 Amp) welding unit

It is used as a power source. Heat generated by the electric arc (~3000 deg C) struck between the electrode and the metals serves to melt the metals placed in the crucible to form an alloy. Repeated melting is performed to improve the homogeneity of the alloy. b) Chiller unit.

The cold circulation water from the chiller cools both the copper hearth and the electrodes.

c) Vacuum unit

It consists of rotary pump which is used to achieve an initial vacuum of 10^{-3} mbar then followed by a vacuum of 10^{-5} mbar which can be achieved by diffusion pump.

Features:

- (i) High melting point metals can be easily melted (note that tungsten is very difficult to melt as it has high melting point (3422 deg C))
- (ii) Improve homogeneity by re-melting 5 to 6 times
- (iii) Inert atmosphere to avoid contamination

2) Induction Levitation Melting (ILM) Unit [16]

Principle:

The copper coil surrounding the metal charge is used to melt the charge by Joules heating. Sample of 10 grams can be easily melted and levitated using vertical component of Lorentz force. Heating rate is faster in ILM unit as heat is produced from inside the sample. ILM unit situated at BARC can produce maximum of 2000-2400 deg C temperature.

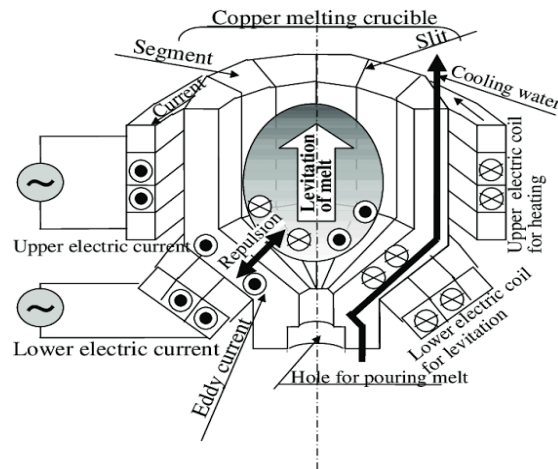


Fig D, Schematics of Levitation Melting unit

Different parts in ILM unit

a) Induction heating power supply unit:

The ILM is powered using a 20 kW, MOSFET-based induction heating unit with an operating frequency of ~ 170 kHz. The inverter is designed for a maximum output voltage of 1000 V.

b) Segmented Copper Crucible:

The segmented crucible has 8 water-cooled fingers, which are arranged to form a

cavity with 20 mm inside diameter. The copper crucible is made of ETP Copper and fabricated from a single extruded ingot. The crucible is housed inside a quartz tube for maintaining adequate vacuum (10⁻³ mbar) using a rotary vacuum pump. The segmented copper crucible is internally water-cooled. the segmented crucible is provided with an appropriate profile from inside to generate adequate vertical component of the Lorentz force and levitate the molten mass to avoid any contamination from the crucible through physical contact. The Lorentz force also results in strong churning action and thereby, a highly homogeneous melt. Thus, the induction levitation melting can be used to prepare ultrapure specimens with high homogeneity.

Advantages of ILM unit over VAM unit

- I. Rapid heating as heat is produced from inside the sample
- II. Better homogeneity can be achieved by churning action that takes place inside the sample during melting by Lorentz force
- III. Less time consuming and ultrapure samples can be prepared

3.1.2. For sample preparation

Cutting

Struers' minitom-10 cutting machine was used to cut all the samples needed for characterization study in which diamond cutter is used to cut the hard samples like W based alloys or Nb based alloys at 150 rpm speed.

Polishing

All the samples were hot mounted in Struers' citropress-5 using condufast powder which is conducting in nature. After hot mounting, all samples had been polished with the help of emery papers and 1-micron alumina powder. Final mirror like polishing was done by colloidal polishing for 1 hour.

3.1.3. For characterization

1. X-Ray Diffraction (XRD) unit

The crystal structure was investigated by using a Bruker D8 discover X-ray diffractometer with Cu K α radiation. The XRD scan angle range was from 20° to 100° at a

scanning rate of 4° per minute. 40 kilo volts was applied to produce x-rays from copper target to get required intensity of K alpha

2. Scanning electron microscopy (SEM) unit

Microstructural and compositional analysis were done using Auriga Carl Zeiss FESEM instrument. In SEM, we used secondary electrons (SE) to get topographic information, back-scattered electrons (BSE) are used to detect Z contrast present in material. For SE and BSE imaging, we used low voltage for electron beam production i.e. 5 KV.

For EDS analysis, we use high voltage to produce electron beam i.e. 20 KV which is necessary for x ray production and 5 mm distance between sample and gun is also maintained. In SEM, high vacuum of the order of 10^{-11} mbar is achieved by rotary, turbo-molecular and ion getter pump which is necessary for better interaction of electrons with sample.

Focus Ion Beam (FIB) technique present in SEM unit is used to prepared site specific samples for TEM analysis. In this technique, firstly, Platinum deposition is done on specific site (which will be used for TEM analysis further) then ions (specially Gallium ions) are used for milling action. Finally, FIB sample of thickness in order of microns is placed on copper grit by using sharp tip needle

3. Transmission Electron Microscopy (TEM) unit

Transmission electron microscopy relies on electrons in a transmission mode rather than backscattering from the sample. For this reason, samples must be electron transparent which equates to a < 80 nm thickness. Producing suitable samples can be very difficult and time consuming, however analysis using this technique is very powerful as high resolution (sub 1-nm) structural and morphological information can be obtained. In the present study, we have used JEOL 2000FX TEM unit to acquire Selected Area Electron Diffraction (SAED) pattern

3.1.4. For synthesis of HEA through powder metallurgy route

1. Ball milling unit

During ball milling, impact, attrition, shear and compression forces are acted upon particles. During impact, striking of one powder particle against another occurs. Attrition refers to the production of wear debris due to the rubbing action between two particles.

Shear refers to cutting of particles resulting in fracture. The particles are broken into fine particles by squeezing action in compression force type.

Mechanism of milling: Changes in the morphology of powder particles during milling

Results in the following events.

1. Microforging, 2. Fracture, 3. Agglomeration, 4. Deagglomeration



Fig E. Schematics of Planetary Ball Mill

2. Hand operated hydraulic press

Compaction is an important step in powder processing as it enables the forming of loose metal powders into required shapes with sufficient strength to withstand till sintering is completed.

In general, compaction is done without the application of heat. Loose powders are converted into required shape with sufficient strength to withstand ejection from the tools and subsequent sintering process. IN cases like cemented carbide, hot compaction is done followed by sintering. One cannot call this as compaction strictly, as sintering is also involved in this



Fig F, Schematics of Hand operated hydraulic press

3. Spark plasma sintering unit

Spark Plasma Sintering is a new technique which takes only a few minutes to complete a sintering process compared to conventional sintering which may take hours or even days for the same. This high sintering rate is possible in SPS since high heating rates can be easily attained due to internal heating of the sample as opposed to external heating seen in case of conventional sintering.

High DC Pulse is passed between graphite electrodes and axial pressure is simultaneously applied from the beginning of the sintering cycle. The sample is heated by the Joule-heating and the sparking among the particles of sintered material leads to the faster heat and mass transfer instantaneously. After the sintering, the power is turned off and the sample is allowed to cool

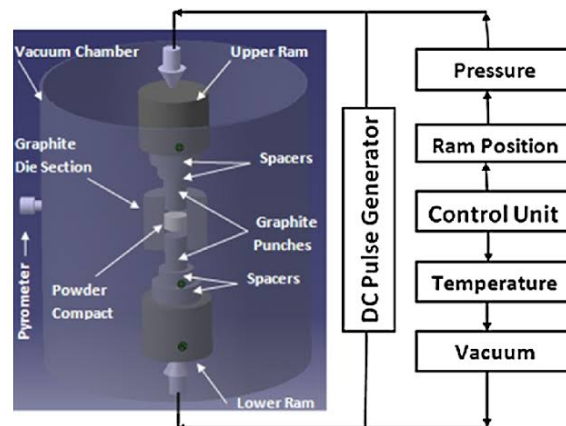


Fig G, Schematics of SPS

3.2. Experimental procedure

3.2.1. For AlZrNbTiV HEA

3.2.1.1. Melting

We have high melting point elements like Nb, V and Ti. Hence, equiatomic AlZr and NbV binary alloys were prepared in levitation melting unit such that their resultant melting point should be lower than high melting point element present in that binary alloy. For example, according to binary AlZr phase diagram, melting point of equiatomic AlZr binary alloy is ~1500 K which is lower than melting point of Zr i.e.2128 K. Finally, we prepared the 25 grams of AlZrNbTiV high entropy alloy by adding Ti in above two binary alloys in levitation melting unit.

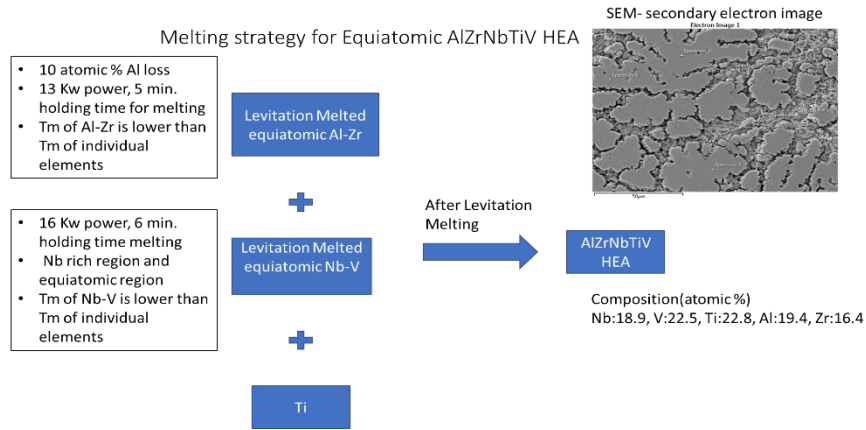


Fig H, Melting strategy for AlZrNbTiV HEA

Compound	Weight of the sample(grams)	Remarks
Equiatomic AlZr	Al=2.28266, Zr=7.717339 Total weight=9.9999	10 atomic % loss of Al confirmed by EDS
Equiatomic NbV	Nb= 5.99556, V=3.287434 Total weight=9.282994	Some Nb-rich regions were observed by EDS
Equiatomic AlZrNbTiV HEA	Zr=7.35825, Al=2.3019(10% extra), Nb=7.479447, Ti=3.861283 and V=4.1092925 Total weight=25.1254	Alloy was melted properly confirmed by SEM analysis

Table 5 Weight of compounds used during melting

Parameters compound	Maximum Power input (Kw) (10% efficiency)	Argon pressure(mbar)	Time given for melting at maximum power input(min)
AlZr	13	300	5
NbV	15	300	5
AlZrNbTiV HEA	16	300	10

Table 6 Parameters used in levitation melting unit

3.2.1.2. Heat treatment

Heat treatment of five samples (sealed in quartz tube with He gas atmosphere) were done for homogenization and to analyzed the microstructural changes like formation of intermetallic, recrystallization and grain growth kinetics, effect on hardness etc.

Following table shows heat treatment of samples for different temperature and time (all samples were furnace cooled)

Temperature (deg C)	950	950	950	950	1200
Time (Hours)	7	15	20	25	24
Heating rate(deg C/min)	10	10	10	10	2

Table 7

3.2.1.3. Characterization

All samples were polished and etched (using 45%HNO₃, 5%HF and 50% H₂O by volume) for further analysis, XRD and TEM (spot SAED patterns) units were used to identify different phases present in the HEA. For compositional and microstructural analysis, we have used Optical Microscope (OM) and SEM techniques. For TEM sample preparation, sample thickness was manually decreased to less than 100 microns, then 3 mm diameter disks were prepared using punching machine. Finally, required thickness was achieved by Jet thinning using an electrolyte comprising 80% methanol and 20% perchloric acid by volume. Vickers micro-hardness unit (Model HPO-250) was used to measured microhardness of the samples by applying a load of 100 grams for 15 seconds.

3.2.2. For WCrMnV HEA

3.2.2.1. Synthesis

A) Melting route

Tungsten has highest melting point around 3422-degree Celsius among all the metals which makes it difficult to melt in vacuum arc melting unit. While, Manganese and Chromium are highly evaporative in nature at high temperatures. Hence, melting of WCrMnV HEA is a difficult task. We melt the WCrMnV HEA in vacuum arc melting unit under Argon atmosphere at 0.5 bar. The melting → solidification → 'turn over' of sample → re-melting process is typically repeated six times for better homogeneity and to melt the tungsten properly. By EDS analysis we have found out that there was loss of Mn and Cr

from alloy. So, we melted the half part of vacuum arc melted sample and MnCr binary alloy in levitation melting. Hence, with the help of Vacuum arc melting unit and levitation melting unit, we were able to prepare WCrVMn high entropy alloy.

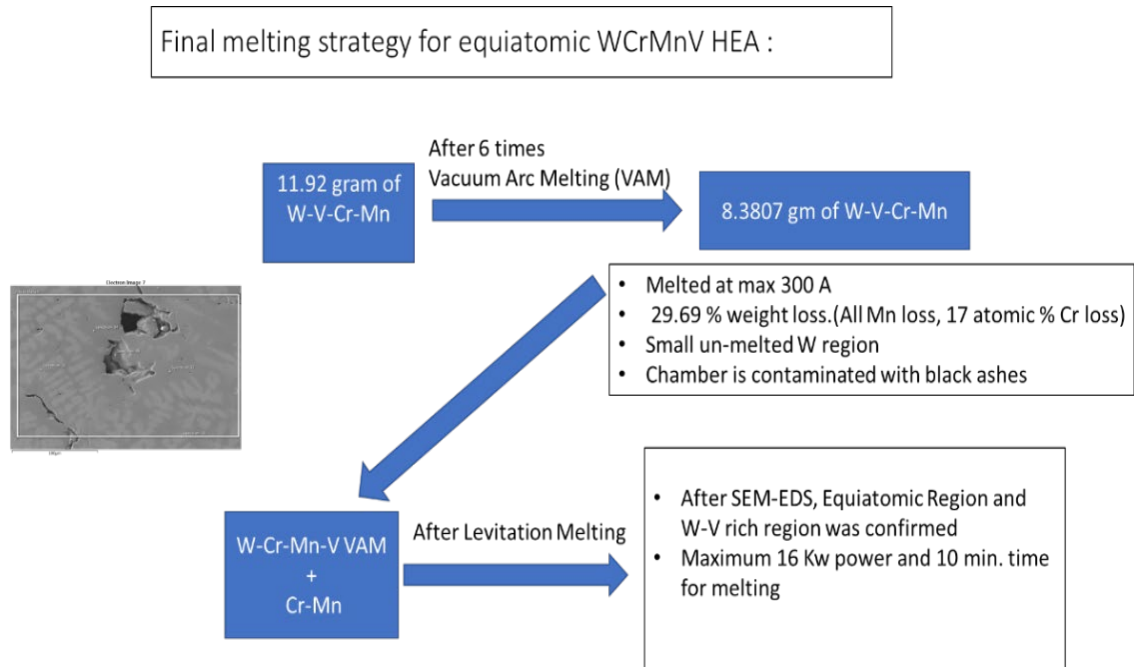


Fig I, final melting strategy for WCrMnV HEA

Compound	Atomic (%)	Weight of the sample(grams) for melting	Remarks
MnV levitation melted	Mn=66.66 V=33.33	Mn=6.8725464(20% extra) V=2.632068 Total weight=9.5045	Successfully melted
WV levitation melted	W=33.33 V=66.66	W=6.33285 V=1.754712 Total weight=8.087562	Un-melted
CrV levitation melted	Cr=50 V=50	Cr=5.373114 V=5.264136 Total Weight=10.637246	Successfully melted
WCrMnV arc melted(6 times remelted)	All are in equiatomic %	W=6.33285 V=1.754712 Cr=1.791038 Mn=2.053(20% extra) Total weight=11.929	SEM analysis was done(showing small

			unmelted W region)
WCrV arc melted with high power	All are in equiatomic %	W=37.66035 V=10.43497 Cr=10.65099 Total weight=58.74631	Un-melted
Small part of equiatomic WCrV arc melted sample was melted in levitation melting		W=6.9201 V=4.9137 Cr=4.6662 Total weight=16.5	Un-melted
WCrMnV arc melted+ MnCr levitation melted equiatomic binary alloy (2 times remelted)		4.28538 g of WCrMnV arc melted + 15 g (CrMn){Cr=7.2 Mn=7.8}	Equiatomic composition was achieved

Table 8 Weight of compounds used during melting

B) Powder route

As it was difficult to prepare WCrMnV HEA through melting route, we have tried to synthesized the HEA by mixing the elemental powder in ball mill (with Toluene as a wet mill agent which act as coolant, hence reducing the chances of formation of oxides) followed by compaction using hand hydraulic press then final densification step was done using conventional sintering and Spark Plasma Sintering (SPS).

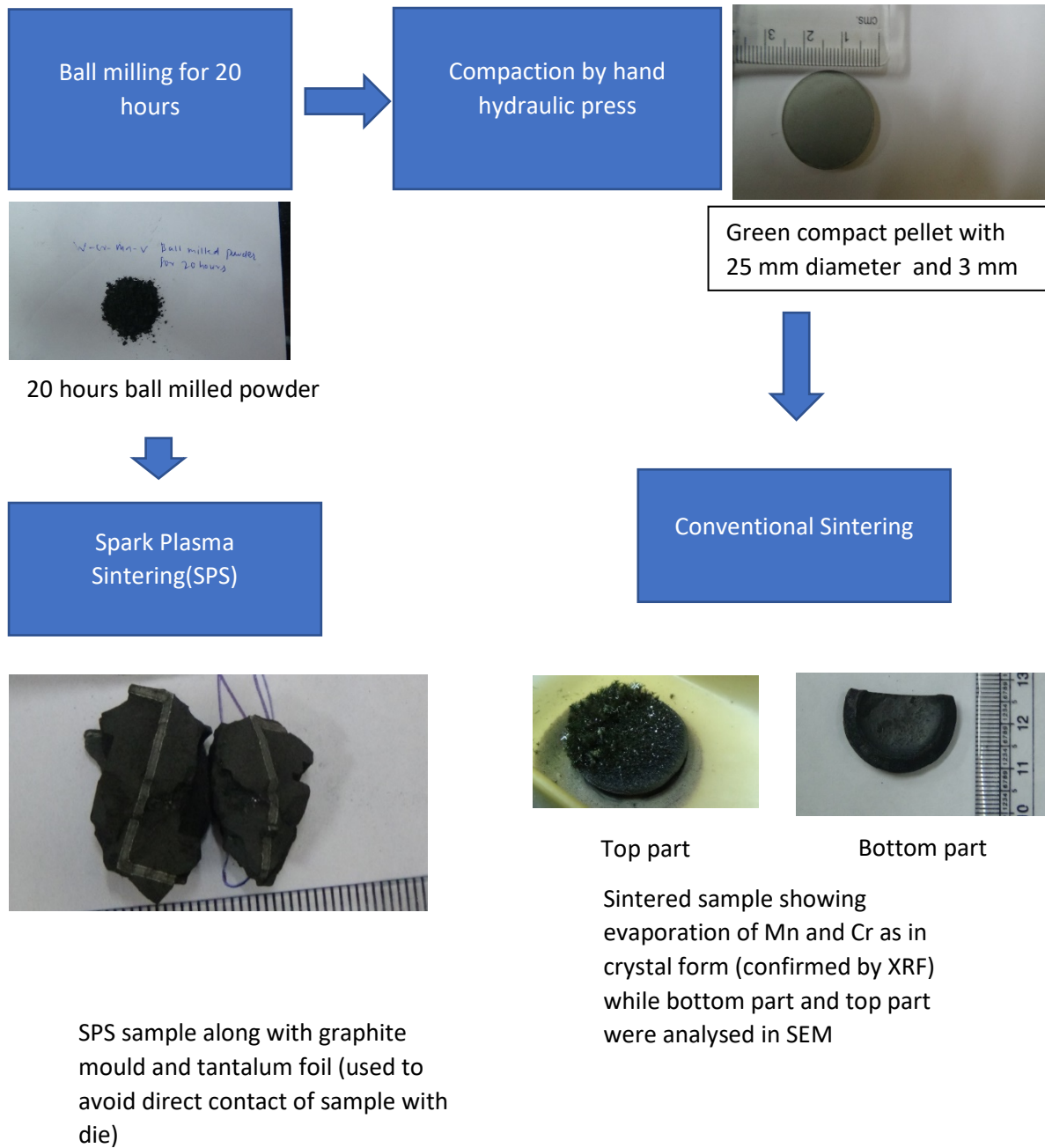


Fig 2 showing powder route for alloy synthesis

B1) Parameters used during synthesis of Equiatomic WCrMnV HEA via powder route

➤ **Parameters for milling**

- Total Weight of the powders= 51.60966 which consist of W=26.90025 g, Cr=7.60785 g, Mn=9.64596 g (20% extra) and V =7.45355 g
- Total weight of the WC balls=700 gram
- Total Weight of the steel pot with WC as an inner lining =3000 g
- Speed of steel pot during milling= 200 RPM

- Total milling time=20 hours (After each one hours 15 minutes break was given)

➤ **Parameters for compaction**

- Pressure used for compaction was 9000 pounds for 2 minutes
- PVB binder was used for better compaction

➤ **Parameters for Conventional sintering**

- Sintering was done in two segments in which sample was first heated to 1200 deg C with 3 deg c/ min as a heating rate. Soak time for 1200 deg C was 2 hours followed by heating at 1500 deg c with same heating rate and soak time as used before.
- Cooling rate was 4 deg c/min

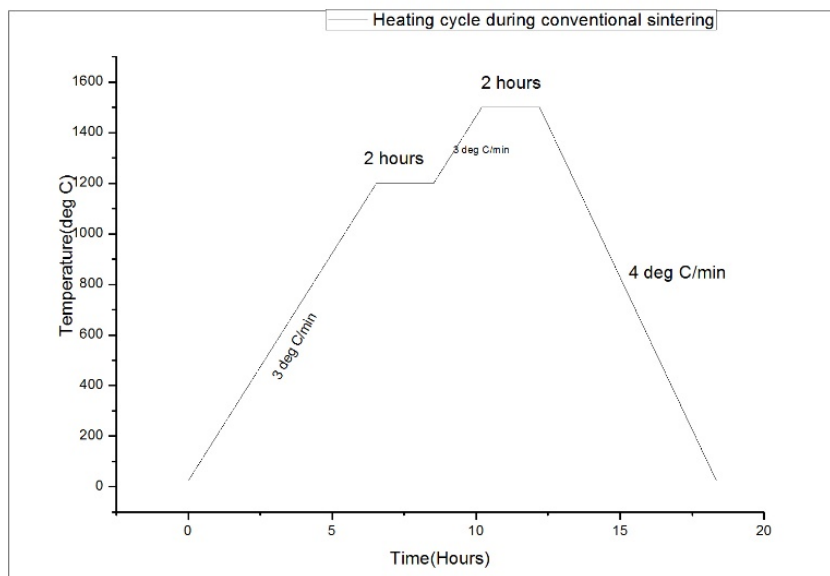


Fig J, Heating cycle during sintering

➤ **Parameters for SPS**

- Weight of milled powder = 15.426 grams
- Heating rate during SPS is 100 deg C/min
- Absolute pressure of chamber during SPS: 0.123 mbar
- Sintering temperature:
 - 1) T1=1100 deg c with 5 minutes as soaking time followed by
 - 2) T2= 1500 deg c with 10 minutes as soaking time
- Pressure given during SPS:
 - 1) Starting from 3KN pressure followed by 6 KN at 1100 deg c for 5 minutes and then 11 KN at 1500 deg c for 10 minutes.
 - 2) Pressure was brought to 0 from 11 KN within 5 minutes.

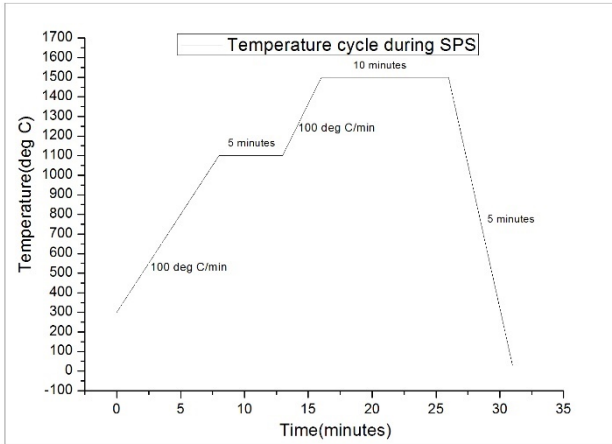


Fig K, temperature variation with time during SPS

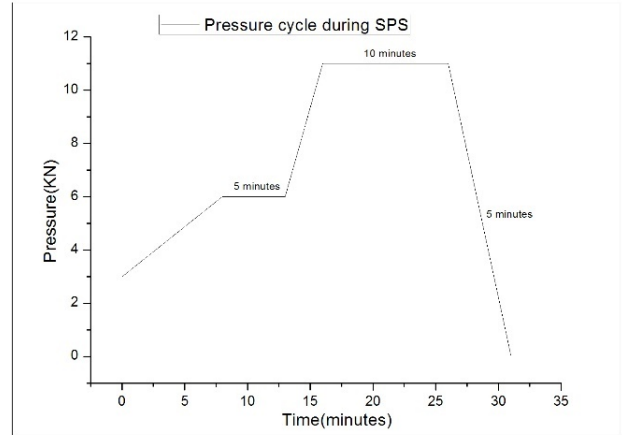


Fig L, pressure variation with time during SPS

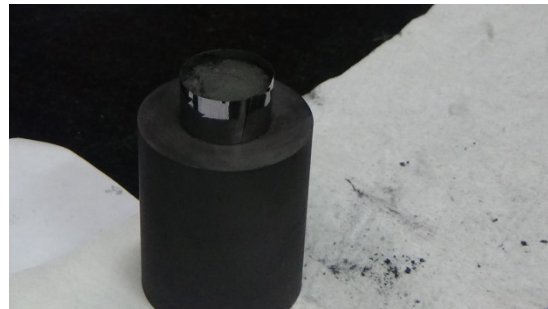
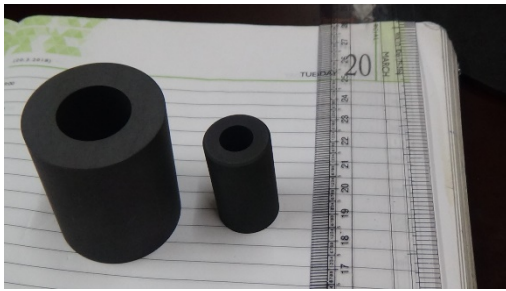


Figure M showing graphite die and two punches used during SPS

3.2.2.2. Characterization

All samples were polished and etched for further analysis. XRD, OM and SEM techniques were used to characterized the sample. Hardness of the sample was measured by Vickers micro-hardness tester.

4 RESULTS AND DISCUSSION

4.1. SEM analysis of Binary alloys

Below figures showing SEM micrograph of binary alloys prepared for final synthesis of AlZrNbTiV and WCrMnV HEAs

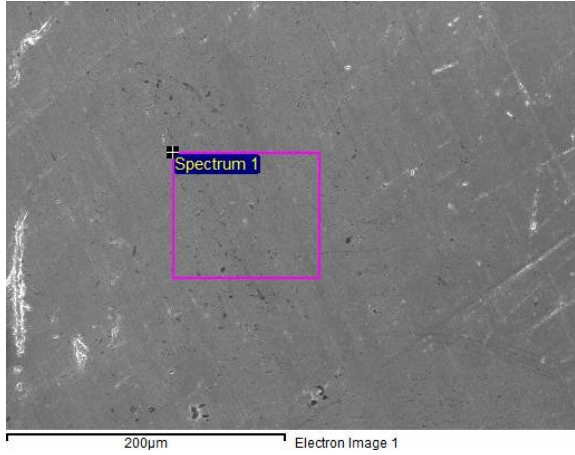


Fig 3(a) showing SEM micrograph of equiatomic AlZr binary alloy

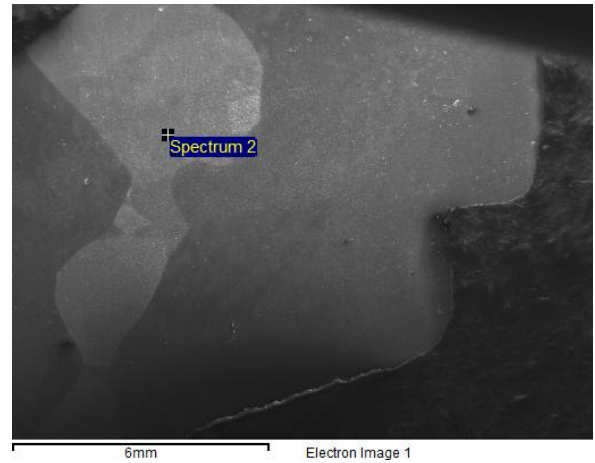


Fig 3(b) showing SEM micrograph of equiatomic NbV binary alloy

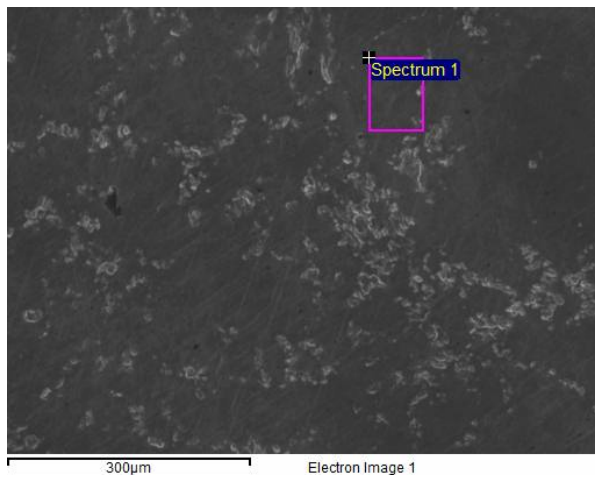


Fig 3(c) showing SEM micrograph of equiatomic MnV binary alloy

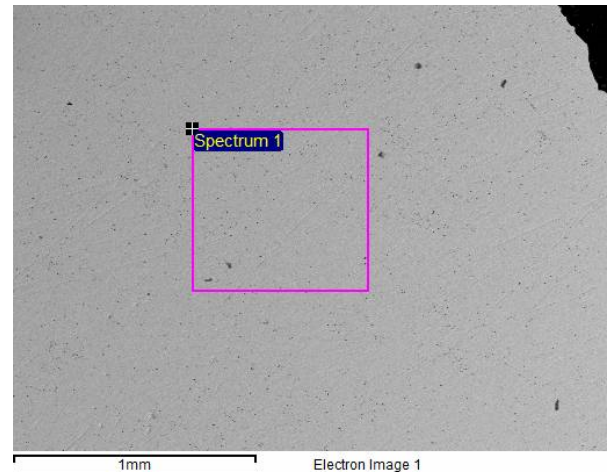


Fig 3(d) showing SEM micrograph of equiatomic VCr binary alloy

Compounds	Composition (atomic %)	
AlZr	Al= 40	Zr=60
NbV	Nb= 91.49	V=8.51
	Nb= 44.48	V=55.22
MnV	Mn=74.22	V=25.78
CrV	Cr= 40.21	V=59.79

Table 9 EDS results of binary alloys

4.2. Characterization of AlZrNbTiV HEA

4.2.1. Characterization of as cast AlZrNbTiV HEA

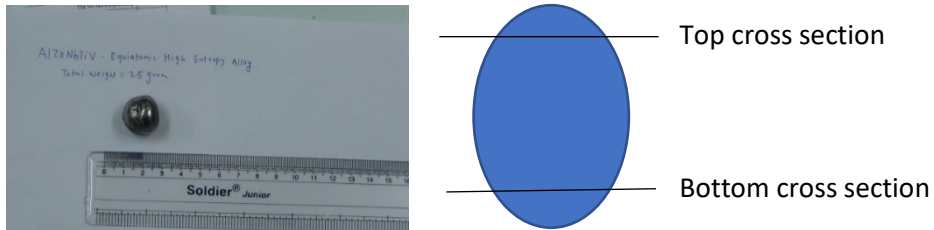


Fig N Levitation melted as cast AlZrNbTiV HEA

A) Top cross section of as cast sample

Fig 4(a) and 4(b) shows optical images of as cast AlZrNbTiV high entropy alloy at different magnification showing dendritic and inter-dendritic region.

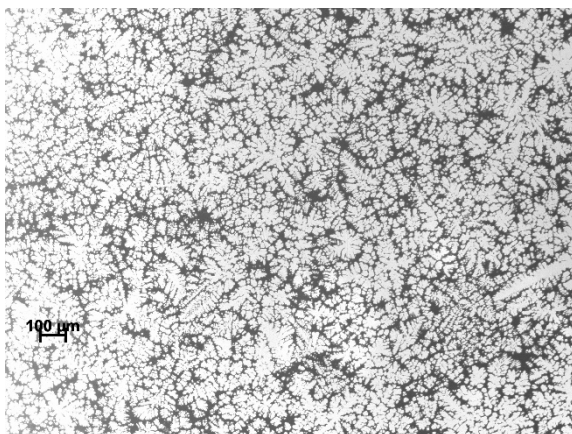


Fig 4(a) at 5X Magnification

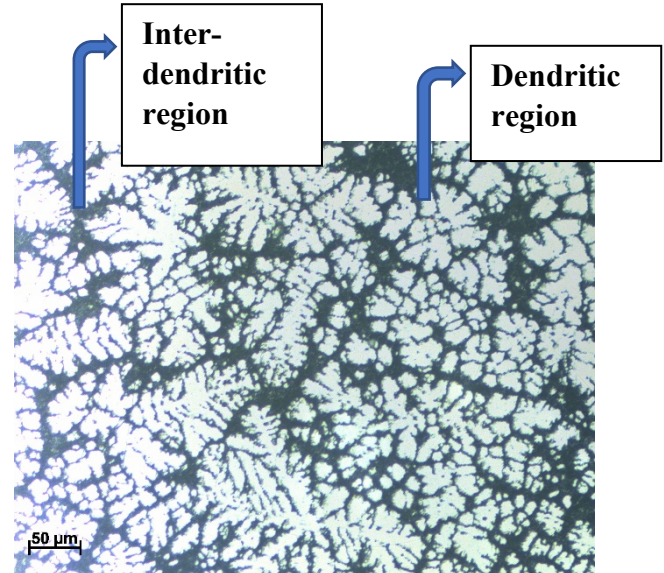


Fig 4(b) at 20X Magnification

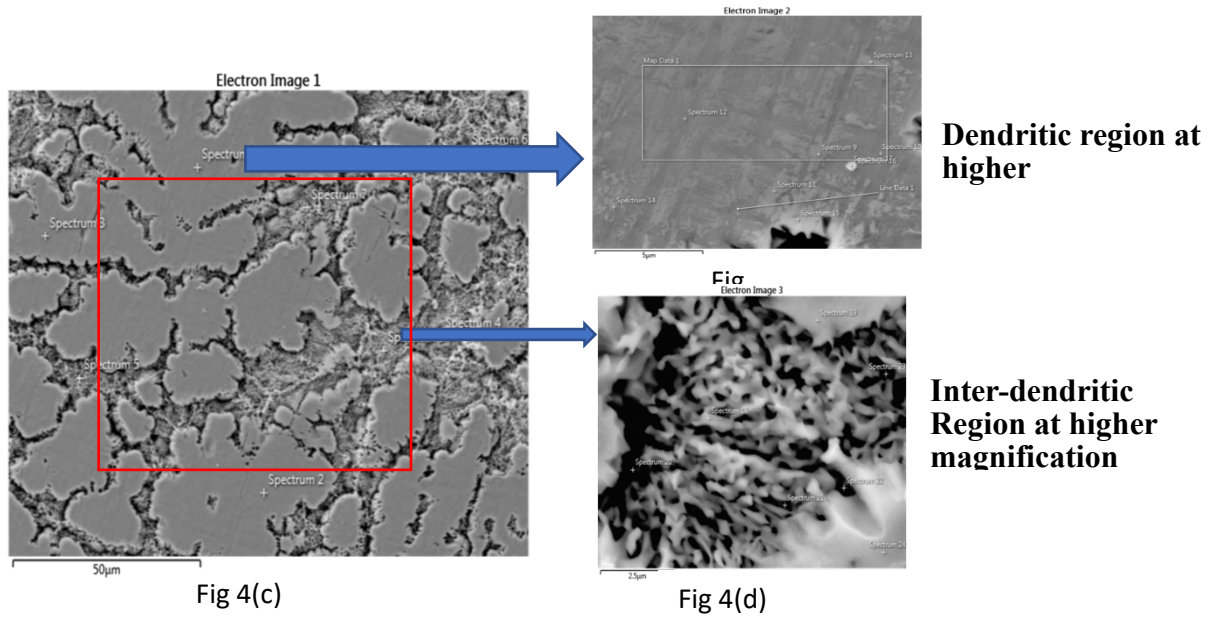


Fig 4(c), 4(d) and 4(e) shows SEM micrograph of the cross section of as cast AlZrNbTiV HEA sample formed by secondary electrons to reveal topographic information.

Elements	Dendritic region(atomic %)	Inter-dendritic region(atomic %)		Map Spectrum(shown in fig 4(c) as a red square)(atomic %)
		White region	Black region	
Nb	29.9 ± 2	23.6±1	19.5±4	25.2
V	20.7 ± 0.3	25.3±1	26.2±4	22
Ti	20.3 ± 0.2	24.4±2	24.1±2	22.7
Al	17.1 ± 0.4	13.8±2	11.2±5	15.4
Zr	12 ± 2	13±2	18.9±5	14.6

Table 10 EDS results of top part of as cast AlZrNbTiV HEA

B) Bottom cross section of as cast sample

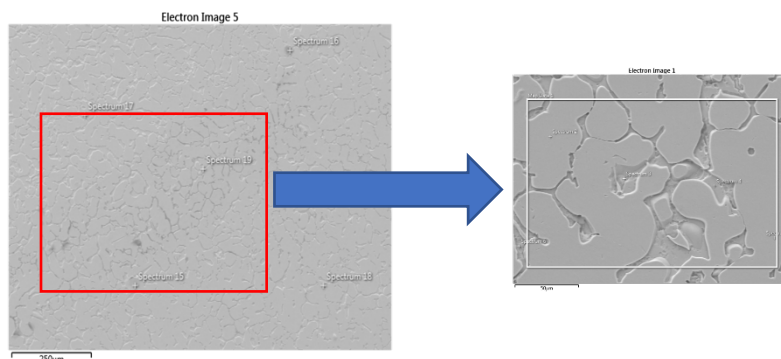


Fig 5 shows SEM micrograph of the bottom cross section of as cast sample

Elements	Dendritic region (atomic %)	Inter-dendritic region(atomic %)	Map spectrum (shown in fig 5 a red square)(atomic %)
Nb	19.8	12.4	18.9
V	21.9	26	22.5
Ti	23.6	14.3	22.8
Al	19.3	22	19.4
Zr	15.5	25.2	16.4

Table 11 Composition of bottom part of as cast AlZrNbTiV HEA

4.2.2. Characterization of Heat treated AlZrNbTiV HEA samples

A) T= 950 deg C for t= 7,15,20,25 hours

Fig 6(a) and 6(b) showing Optical images for sample heat treated at 950 deg c for 7 hours

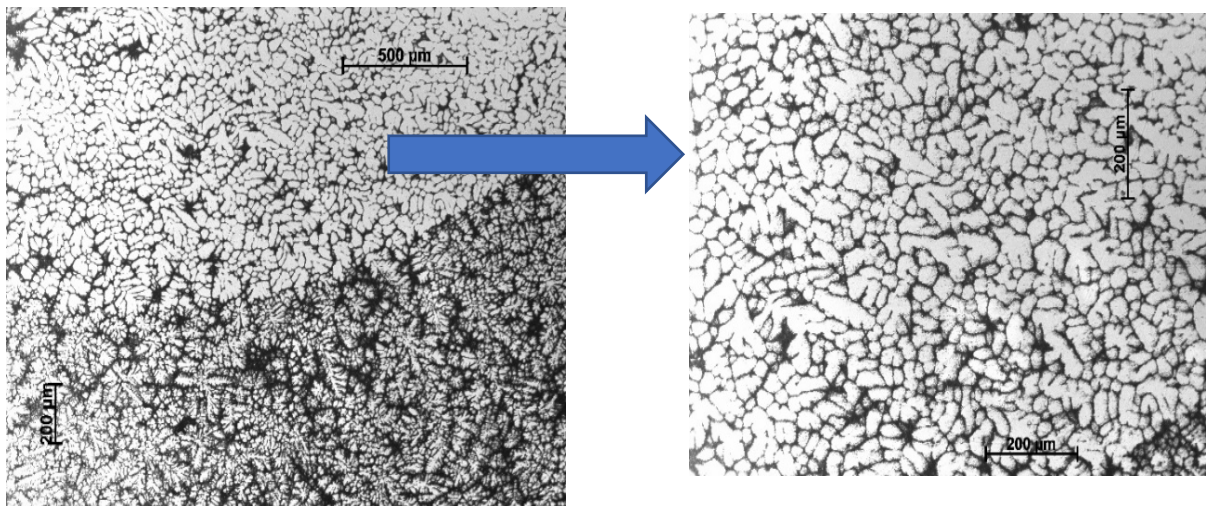


Fig 6(a) at 5x magnification (950 deg C for 7 hours)

Fig 6(b) at 20x magnification (950 deg C for 7 hours)

Fig 7(a),7(b) and 7(c) showing SEM images of heat-treated samples at 950 deg c for 15,20,25 hours

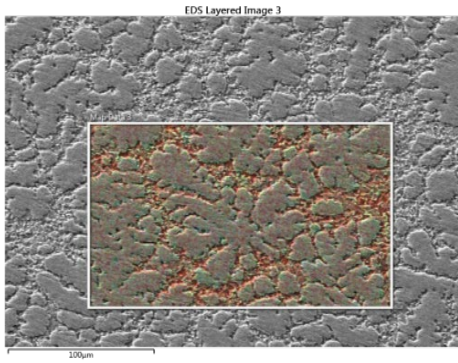


Fig 7(a) showing SEM micrograph

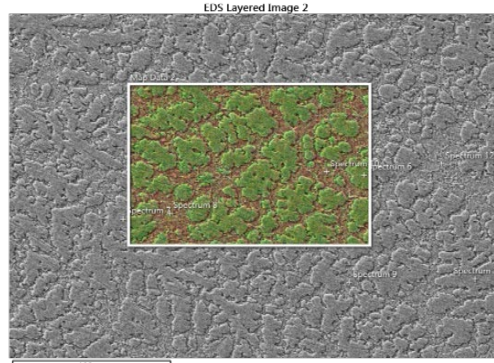


Fig 7(b) showing SEM micrograph

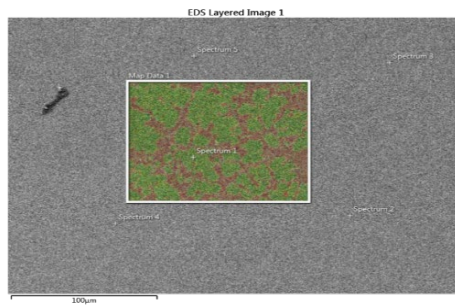


Fig 7(c) showing SEM micrograph

Map composition(atomic%)	Al	Zr	Nb	Ti	V
As cast sample	15.4	14.6	25.2	22.7	22
Sample heat treated at 950 deg c for 15 hours	17.5	17.8	23.5	20.7	20.7
Sample heat treated at 950 deg c for 20 hours	20.6833	21.3833	21.7666	18.3166	17.8166
Sample heat treated at 950 deg c for 25 hours	21.1	22.1	20.4	18.1	18.4

Table 12(a) Map composition of heat-treated samples at 950 deg C for 15,20,25 hours

	950 deg c for 20 hours		950 deg c for 25 hours	
	Dendritic region(atomic%)	Inter-dendritic region(atomic%)	Dendritic region(atomic%)	Inter-dendritic region(atomic%)
Al	17.4	23.7	17.7	28.3
Zr	13.6	31.8	14.6	33.8
Nb	28.2	13.9	25.5	12.1
Ti	20.4	15.3	20.7	10.5
V	20.4	15.2	21.5	15.3

Table 12(b) Point composition of heat-treated samples at 950 deg C for 20,25 hours

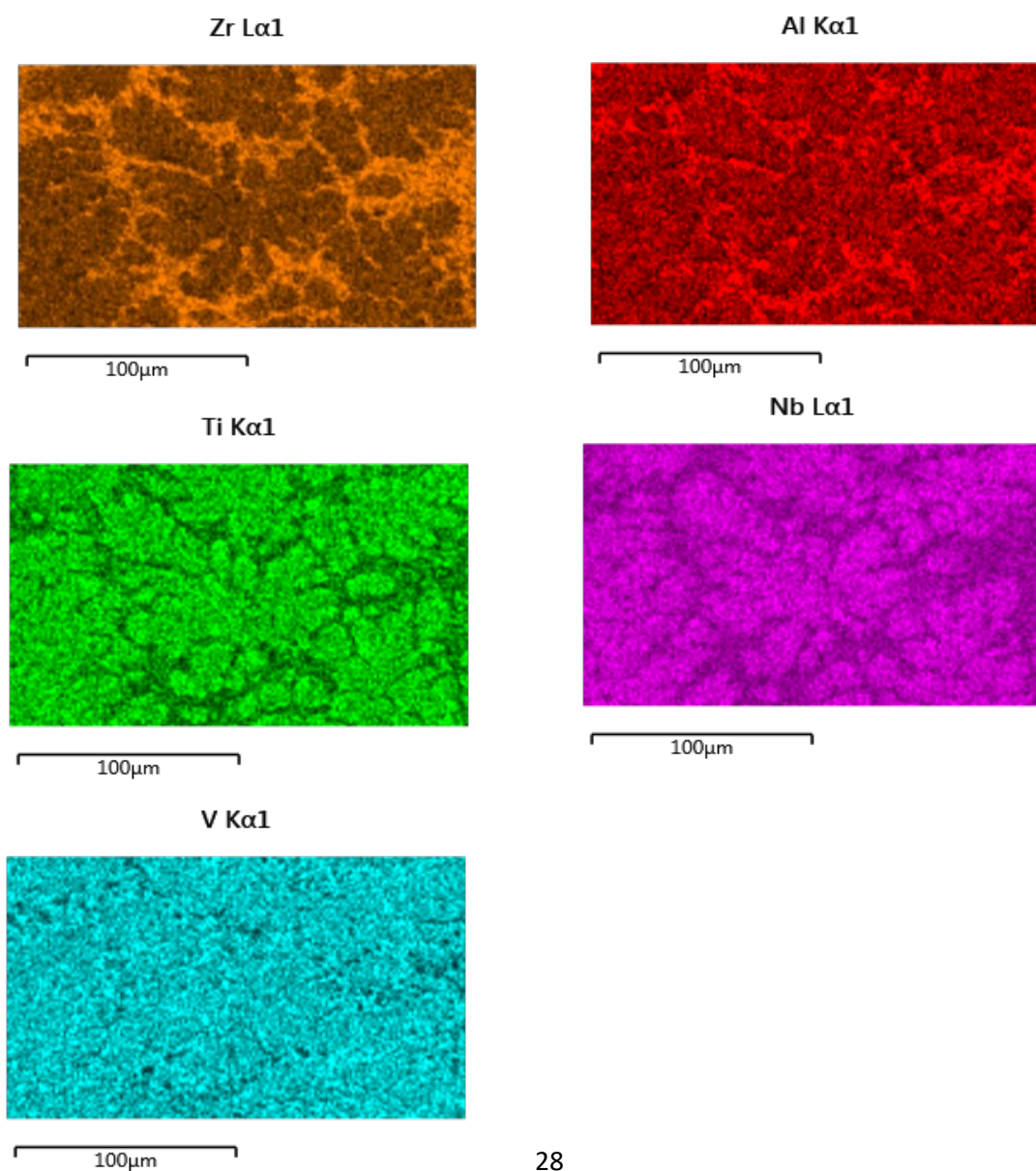


Fig 8 showing Map spectrum of individual elements of heat-treated sample at 950 deg c for 15 hours(fig 7(a)) showing Zr and Al are rich at inter-dendritic region while dendritic regions are rich in Nb and Ti. V is almost evenly dispersed throughout the map spectrum (Samples heat treated at 950 deg c for 7,20 and 25 hours shows the similar distribution of elements in map spectrum (map regions are shown as a square box in fig 7(a),7(b) and 7(c))

B) T=1200 deg C for t=24 hours

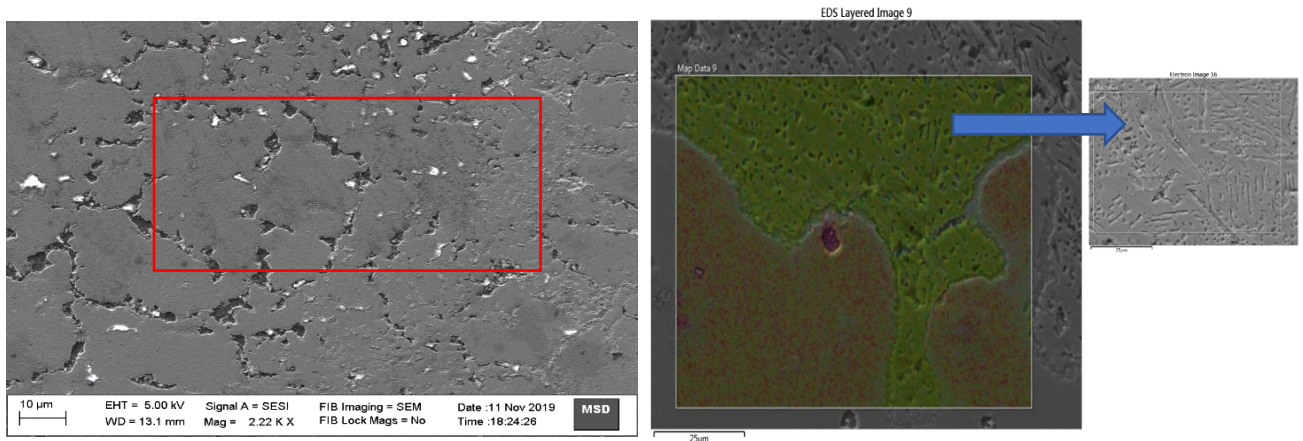
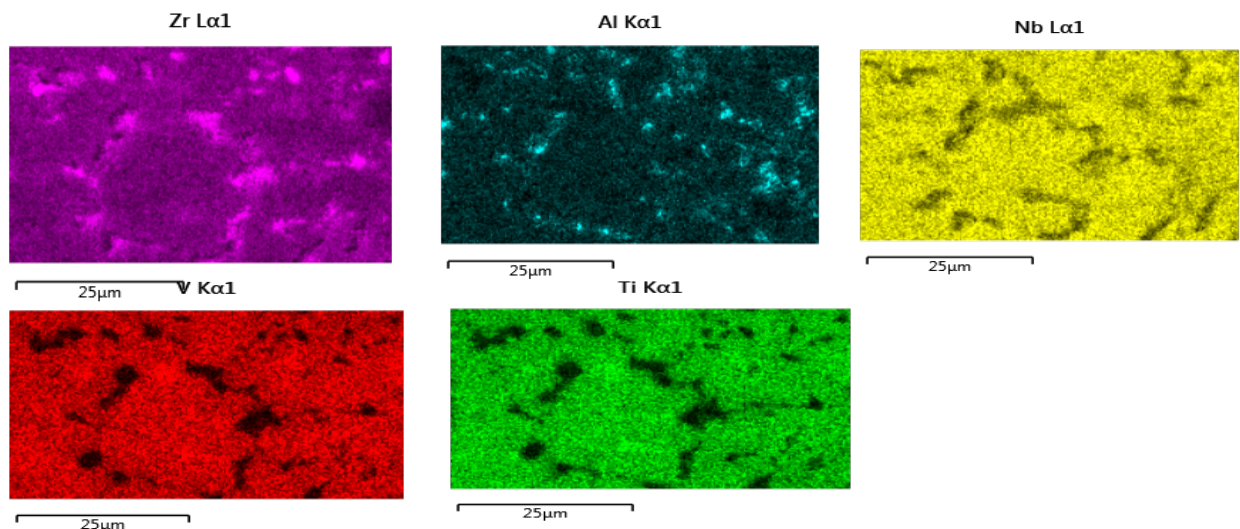


Fig 9 showing SEM micrograph of heat-treated sample at 1200 deg c for 24 hours

Composition (atomic%)	Grain region	Grain boundary region		Map spectrum
		Region 1	Region 2	
	Nb	19.9	4.9	5.7
V	17.2	1.9	3.4	16
Ti	27.1	4.5	6.5	23.7
Al	5.3	20.1	9.3	7.8
Zr	30.6	68.6	75	35.6

Table 13 Composition of heat-treated sample at 1200 deg C for 24 hours

Fig 10, Map spectrum of individual elements of heat-treated samples at 1200 deg c for 24 hours(fig 9, rectangular box) showing Zr and Al are rich at grain boundary region while grain regions are rich in Nb, Ti and V



4.2.3. Crystal structure of as cast AlZrNbTiV HEA

4.2.3.1. XRD of as cast samples

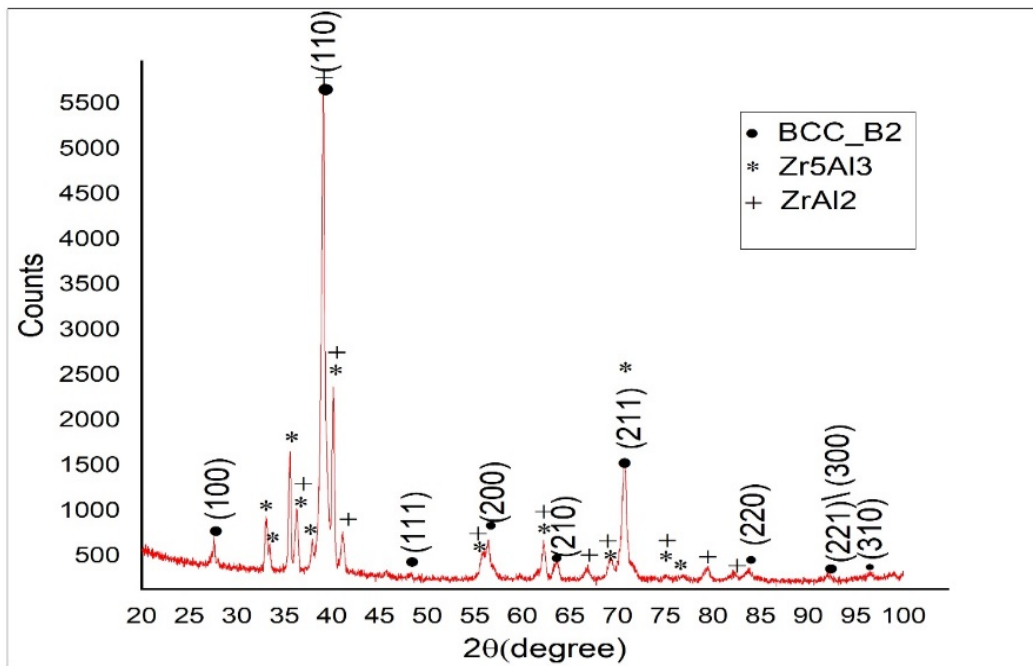


Fig 11 shows the XRD pattern of the top cross section of as cast AlZrNbTiV HEA sample.

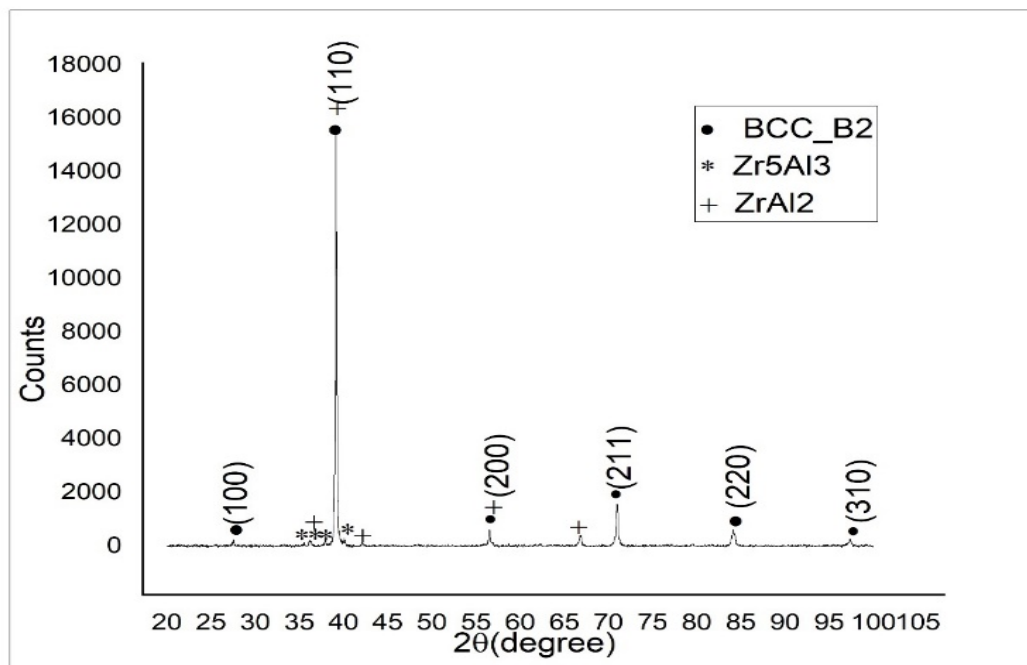


Fig 12 shows the XRD pattern of the bottom cross section of as cast AlZrNbTiV HEA sample.

4.2.3.2. TEM of as cast AlZrNbTiV HEA

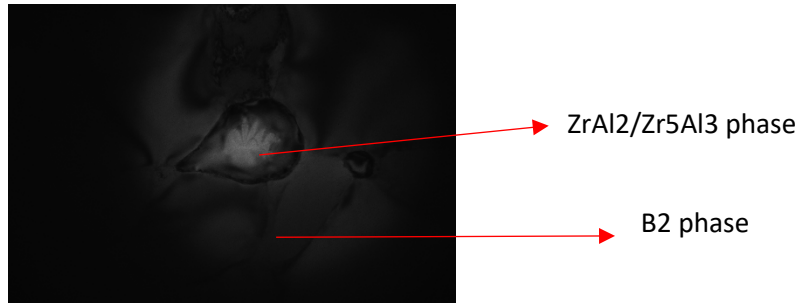


Fig O shows TEM micrograph showing brightfield image at 25K magnification

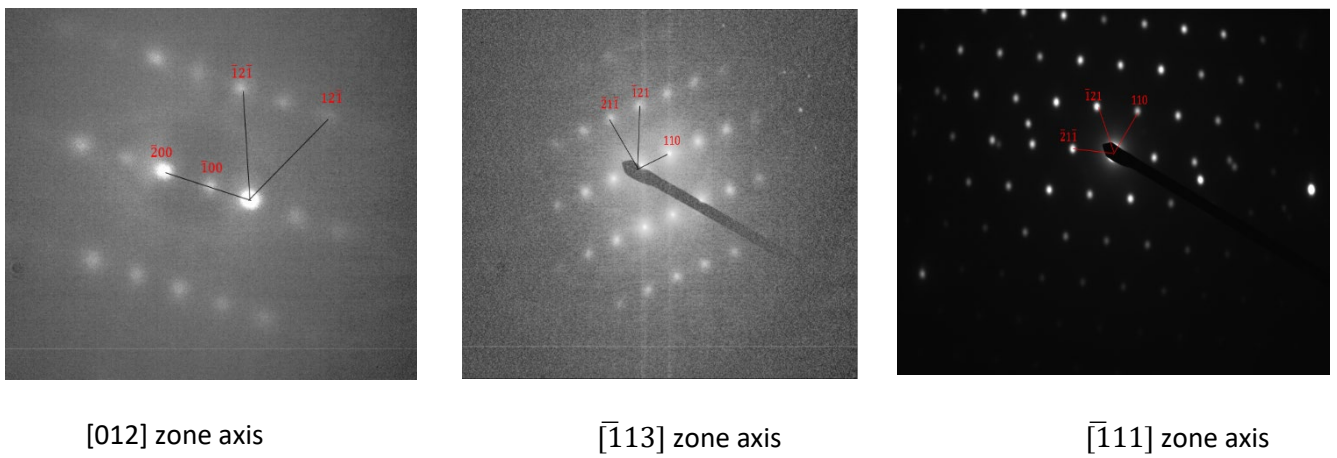


Fig P shows Spot electron diffraction patterns (SAED) along three different zone axes ($[012]$, $\bar{1}13$ and $\bar{1}11$) of B2(Ordered BCC) phase.

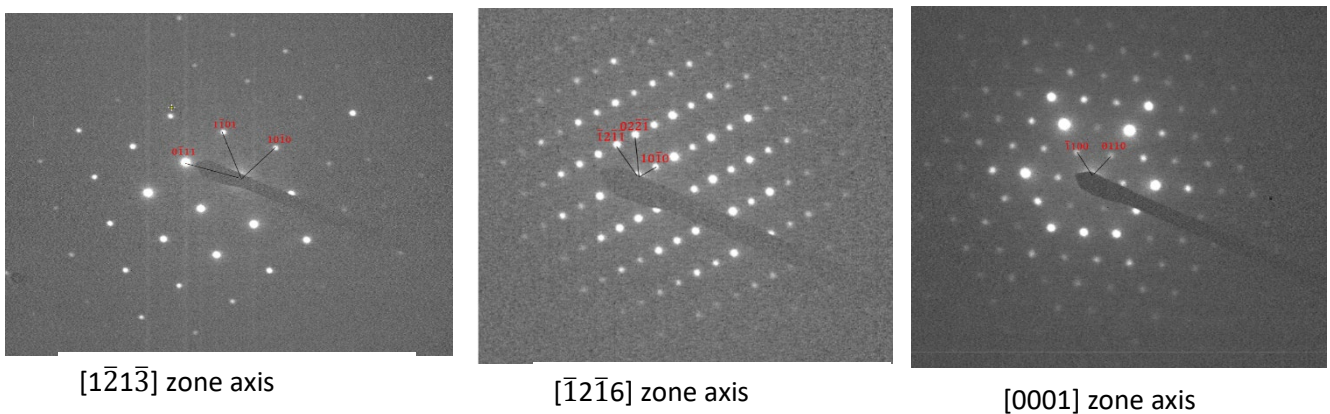


Fig Q shows Spot electron diffraction patterns (SAED) along three different zone axes ($[1\bar{2}1\bar{3}]$, $[1\bar{2}1\bar{6}]$ and [0001]) of hexagonal crystal structure.

4.3. Micro-hardness of AlZrNbTiV HEA

Vickers micro-hardness tester LM 300 AF was used with square based pyramidal indenter to calculate micro-hardness at 100 g load for 15 seconds

Vickers micro-hardness is given as

$HV = \text{force of indentation} / \text{projected area of indentation}$

where area is calculated from square diagonals

Sample	HV1	HV2	HV3	HV average
As cast	589.2	559.8	580	576.3333
Heat treated at 950 deg c for 15 hours	597.2	601.7	567.9	588.933
Heat treated at 950 deg c for 20 hours	642.7	602.7	607.9	617.766
Heat treated at 950 deg c for 25 hours	692.4	691.5	689.4	691.1
Heat treated at 1200 deg c for 24 hours	860.5	1040.4	1181	1027.3

Table 21 Microhardness of AlZrNbTiV HEA

4.4. Discussion on AlZrNbTiV HEA

- Average composition of the bottom and top part of the sample is Nb:18.9, V:22.5, Ti:22.8, Al:19.4, Zr:16.4 and Nb:25.2, V:22, Ti:22.7, Al:15.4, Zr:14.6 respectively which is approximately in equiatomic proportion. There was loss of Al and Zr during melting which can be infer from above composition, this is because of their high vapor pressure compare with other elements in alloy at high temperatures [14].
- Dendrite regions shown in fig 4(c) were found lean in Zr and rich in Nb content (Table 10 and 11). On the other hand, inter-dendritic regions were found to be rich in Zr and lean in Nb content. In inter-dendritic regions, we have found out different compositions of white and black region as mention in table 10. This difference of Zr an Nb composition in dendritic and inter-dendritic regions is owing to the positive enthalpy of mixing between Zr and Nb which means they hate each other and hence tends to separate from each other.
- In order to identify phases and cooling effect on phase fraction, XRD was carried out on top and bottom cross-section of the AlZrNbTiV HEA sample with Cu K α radiation. Fig. 11 and 12 shows the XRD patterns acquired from top and bottom cross section of the sample respectively. The XRD patterns of both cross sections can be indexed in terms of ordered body centered cubic B2 phase (which shows Principle peaks (110), (200) etc. and strong superlattice peak (100) at $2\theta=27.6182$ among other superlattice peaks (111), (210) etc.) with lattice parameter of 0.32628 nm as a major phase (dendritic region) and intermetallic(s) in inter-dendritic region as minor phase(s) can be best indexed with Hexagonal Zr₅Al₃-type(space group-P63/mcm(193) and lattice parameters of a:8.184 Å, c: 5.702 Å) and Hexagonal ZrAl₂-type (space group-P63/mmc and lattice constant of a: 5.282 Å, c:8.748 Å) [7].
- Bottom part of the sample was closed to the water-cooled copper hearth, Hence, was cooled faster than top part of the sample. From peak intensities, we can deduce that bottom part of the sample almost has single order BCC_B2 phase. Hence By controlling the critical cooling rate, we can achieve single phase.
- TEM of as cast AlZrNbTiV HEA was done, Spot electron diffraction patterns at three different zone axes for B2 and hexagonal phase (ZrAl₂ and Zr₅Al₃) as shown in fig O, P and Q was indexed properly which support the result obtained from XRD technique
- SEM micrographs of heat-treated samples at 950 deg C for 7,15,20,25 hours show same microstructure as cast structure (dendritic and inter-dendritic regions). By EDS analysis,

we have confirmed that inter-dendritic regions were Zr and Al rich while Nb and Ti were rich in dendritic regions and V was homogenized throughout the sample (Table 12(a) and 12 (b))

- SEM micrograph of heat-treated sample at 1200 deg C for 24 hours shows recrystallized structure, From EDS analysis, we have confirmed that grain boundary regions were almost rich in Zr and Al content with two different compositions (Table 13)
- From the heat treatments at different temperatures and times, we have confirmed that as you increase the temperature or time, inter-dendritic regions show the increase in Zr and Al content while dendritic regions shows the increase in Nb , Ti and V content
- From table 21, Vickers micro-hardness values for as cast sample, heat treated samples at 950 deg c for 15,20,25 hours and heat-treated sample at 1200 deg c for 24 hours are 576.33, 588.933, 617.766, 691.1 and 1027.3 respectively.
- Micro-hardness does not increase significantly after homogenization of as cast sample at 950 deg C for 15, 20 and 25 hours. But, drastically increase in micro-hardness was observed when as cast sample was homogenized at 1200 deg C for 24 hours as fraction of intermetallics increases in sample which results in dislocation pinning around them, hence, microhardness increases [16].

4.5 Characterization of WCrMnV HEA

4.5.1. Arc melted WCrMnV HEA

Fig 13(a) and 13(b) shows SEM micrograph of arc melted WCrMnV HEA which shows dendritic and interdendritic region along with small region of unmelted tungsten. Composition(atomic %) of dendritic and interdendritic region is shown in table 15 while table 16 shows composition of unmelted tungsten.

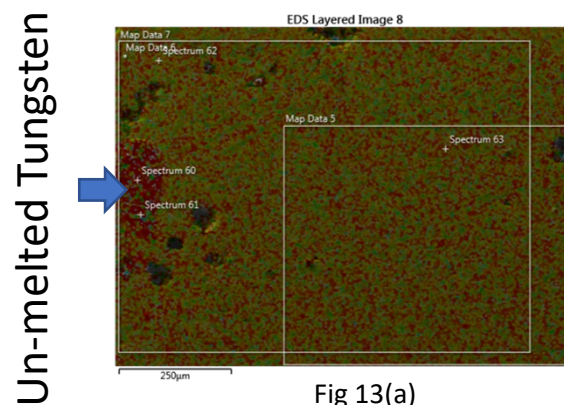


Fig 13(a)

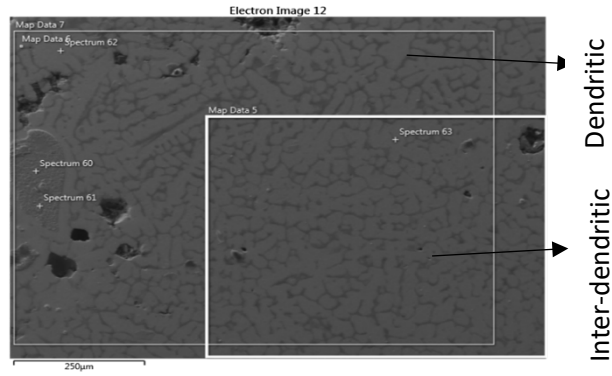


Fig 13(b)

Composition(atomic%)	Dendritic region	Inter-dendritic region	Map spectrum(map data 7 as shown in fig 13(b))
W	61.9	12	42.1
Cr	6.6	19.4	16.4
Mn	0.5	0.3	0.2
V	31	68.3	42.3

Table 15 Composition of arc-melted WCrVMn HEA

Elements	Spectrum 60(atomic%)
W	99.3
Cr	0.7
Mn	0
V	0

Table 14 Composition of un-melted WCrVMn HEA

4.5.2. Levitation melted WCrMnV HEA

Fig 14 (a), (b) and (c) shows the SEM micrograph of levitation melted WCrMnV HEA and table 17 and 18 gives their composition information(atomic%). MnCr binary region is shown in fig 14(c) and main WCrMnV HEA region is shown in fig 14(b) which reflects nearly equiatomic region (Grey region) and tungsten and vanadium rich region (white region)

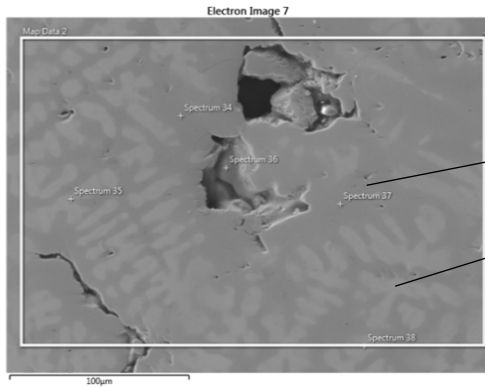


Fig 14(b)

Elements	Grey region	White region
W	18.5	62.4
V	31.4	33.4
Cr	25.3	3.5
Mn	24.8	0.7

Table 16

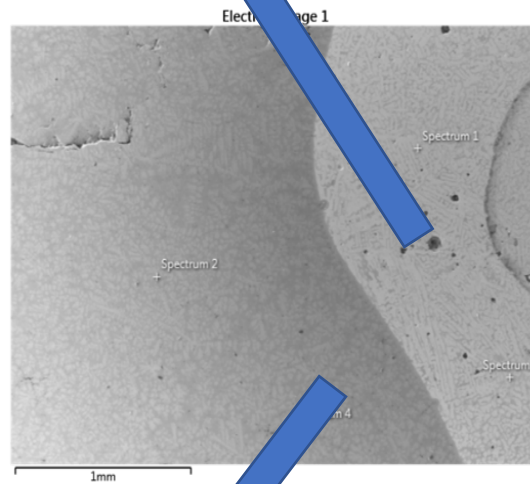


Fig 14(a)

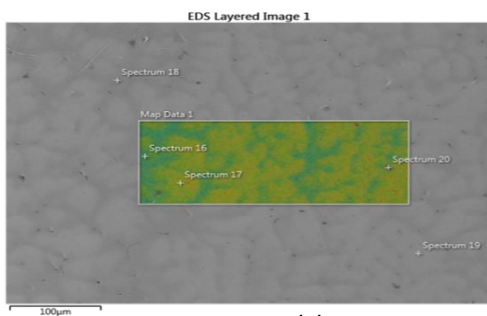


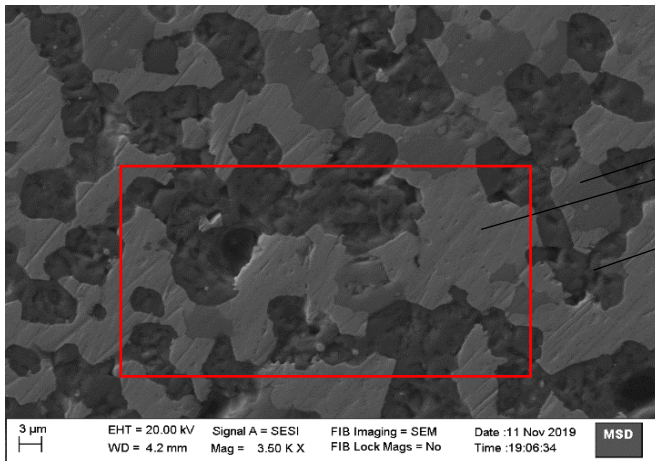
Fig 14(c)

Elements	Map spectrum
W	4.1
Cr	50.4
Mn	40.8
V	4.6

Table 17

4.5.3. Conventional sintered WCrMnV HEA

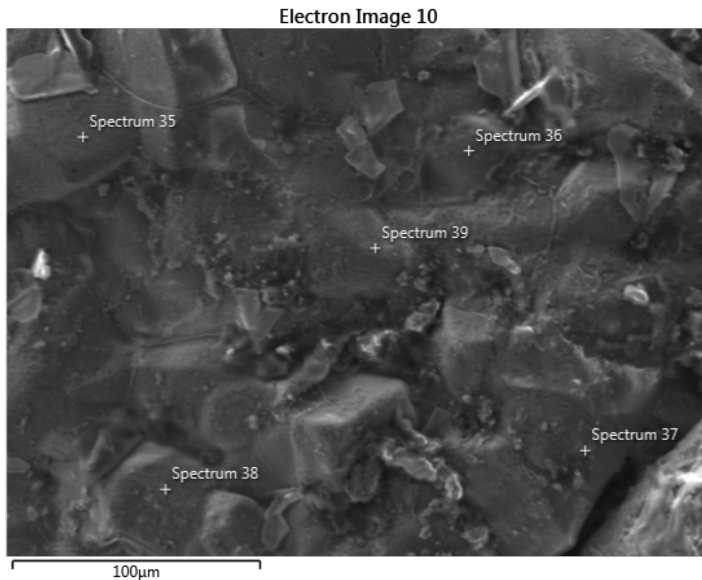
Fig 15(a) and (b) shows the SEM micrograph of bottom and top part of conventional sintered WCrMnV HEA respectively. Bottom part contains three different regions namely region 1 which is W,Cr and V rich ,region 2 which is W rich and region 3 which is an oxide of Cr,Mn and V as shown in table 18. Top part is mainly consisting of Manganese oxides (table 19)



Composition (atomic%)	Region 1	Region 2	Region 3	Map spectrum
W	43.1	89	0.2	23.9
Cr	21.8	5.6	8.1	18.6
Mn	1.5	1.2	15.2	18.2
V	33.6	4.1	24.7	39.6
O			51.8	

Fig 15(a), Bottom part

Table 18



Composition (atomic%)	Region 1
W	0.5
Cr	5.9
Mn	66.3
V	5.6
O	21.8

Fig 15(b), Top part

Table 19

4.5.4. Spark plasma sintered WCrMnV HEA

Fig 16 shows the SEM micrograph of spark plasma sintered WCrMnV HEA which contains three different regions namely region 1 which is W rich, region 2 which is W,Cr and V rich and region 3 which is an oxide of Cr,Mn and V as shown in table 18

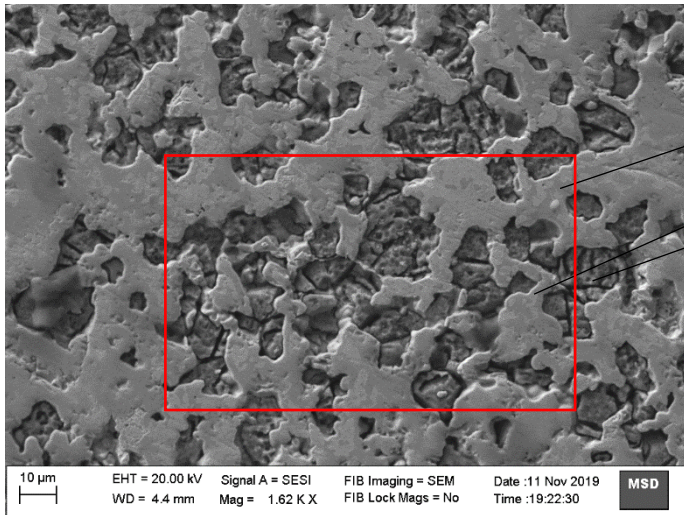


Fig 16

Composition (atomic%)	Region 1	Region 2	Region 3	Map spectrum
W	83.4	35.1	4.3	27.2
Cr	7.4	24.3	7.7	17
Mn	3.2	6.8	47.7	32.2
V	5.9	33.8	13	23.6
O			27.3	

Table 20

4.5.5. Crystal structure of WCrMnV HEA

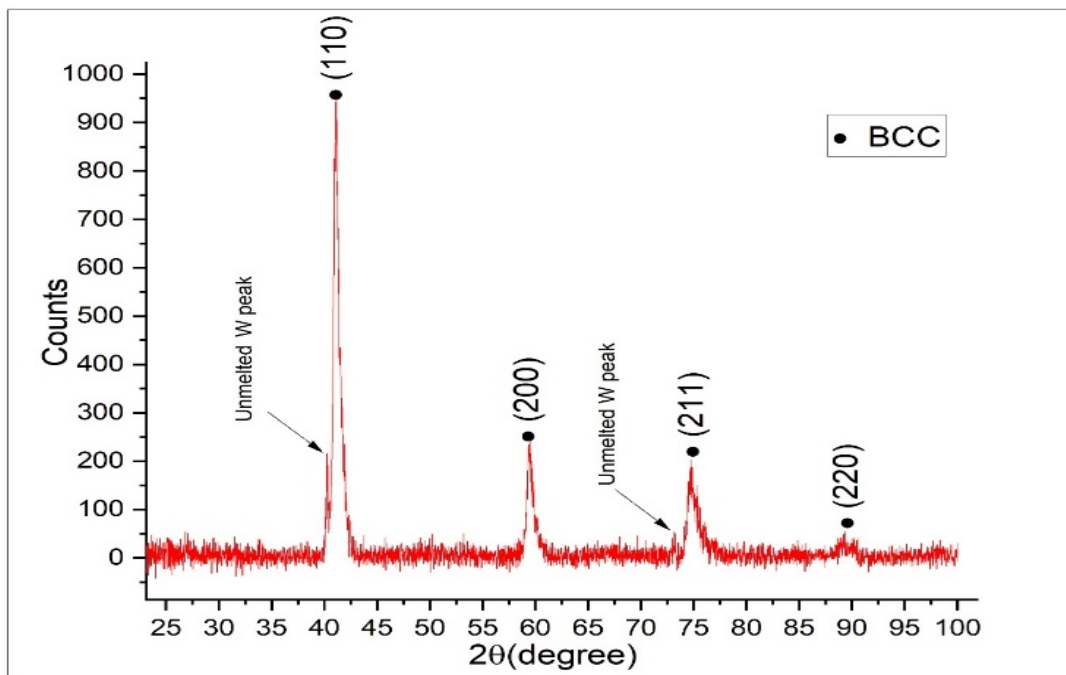


Fig 17(a) shows the XRD graph of WCrMnV arc melted sample

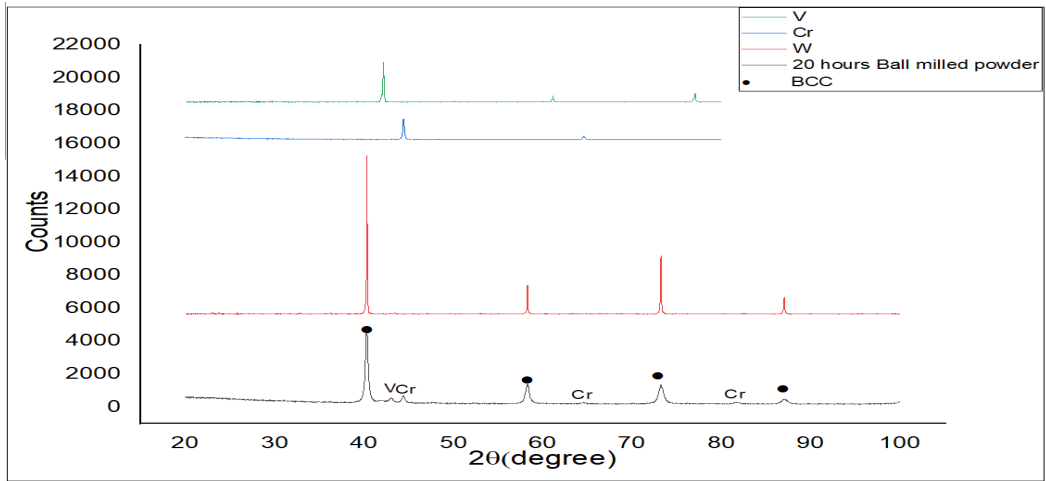


Fig 17(b) shows the XRD graph of W,Cr,V powders and 20 hours Ball milled WCrMnV powder

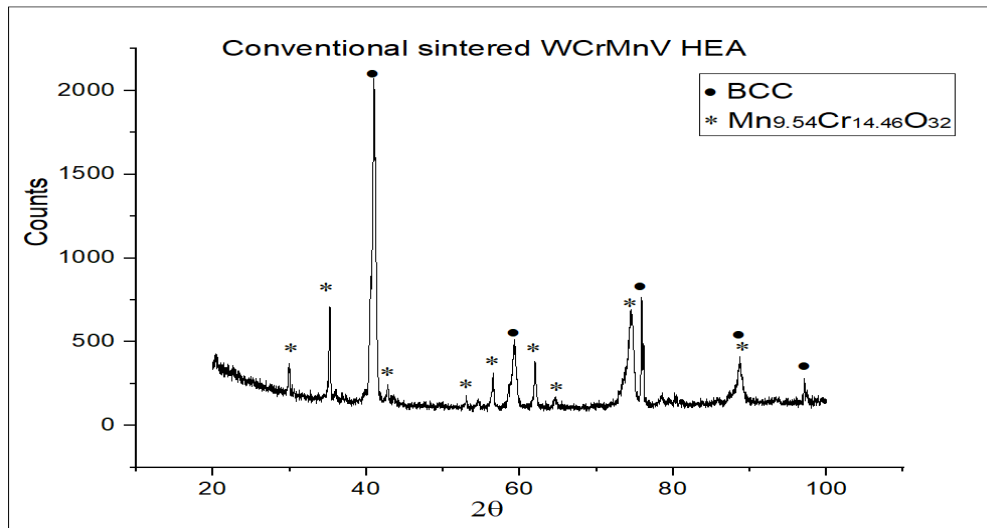


Fig 17(c) shows the XRD graph of back side of WCrMnV conventional sintered sample

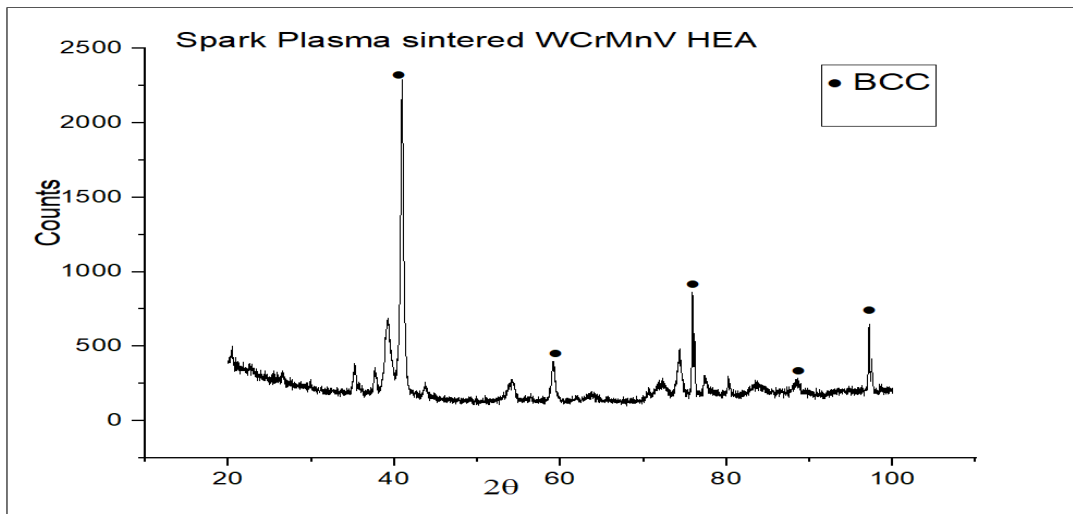


Fig 17(d) shows the XRD graph of WCrMnV spark plasma sintered sample

No.	Pos. [°2Th.]	BCC pekas with lattice constant of 3.103542985 A
1	40.2998	
2	41.1464	1 1 0
3	59.4812	2 0 0
4	73.1895	
5	74.8156	2 1 1
6	89.266	2 2 0

Table 21 show peaks of BCC phase with lattice constant of 3.1035429 A for arc melted WCrMnV HEA

No.	Pos. [°2Th.]	(hkl) for BCC with lattice constant of 3.16534459 A
1	40.2875	1 1 0
2	43.0292	
3	44.4103	
4	47.8642	
5	58.2814	2 0 0
6	64.6097	
7	73.2476	2 1 1
8	81.7652	
9	87.0948	2 2 0

Table 22 show peaks (hkl) of BCC phase with lattice constant of a=3.16534459 for 20 hours ball milled powder of WCrMnV HEA

No	Pos. [°2Th.]	(hkl) for BCC with lattice constant of 3.119671162 A	(hkl) for Cr9.54Mn14.46O32
1	29.9223		1 1 1
2	35.2172		0 2 2
3	41.0165	1 1 0	
4	42.7808		0 4 0
5	53.0179		2 4 2
6	56.4932		1 5 1
7	59.3153	2 0 0	
8	62.0015		0 4 4
9	64.5826		1 5 3
10	74.5181		2 6 2
11	75.8955	2 1 1	
12	88.6855	2 2 0	1 7 3
13	97.133	3 1 0	

Table 23 show peaks (hkl) of BCC phase (a=3.11967 A) for conventional and spark plasma sintered WCrMnV HEA and Cr9.54Mn14.46O32 phase for conventional sintered WCrMnV HEA (note that SPS WCrMnV HEA shows some unidentified phase(s) which is(are) not indexed yet)

4.6. Microhardness of conventional sintered WCrMnV HEA

Vickers microhardness tester LM 300 AF was used with square based pyramidal indenter to calculate microhardness at 100 g load for 15 seconds

Vickers microhardness is given as $HV = \text{force of indentation} / \text{projected area of indentation}$ where area is calculated from square diagonals

Vickers hardness (HV) for Sintered samples is 700.36666

HV1	HV2	HV3	HV average
752.3	744.7	604.1	700.36666

4.7. Discussion on WCrMnV HEA

- After 6 times melting of WCrMnV HEA in vacuum arc melting unit, we have found out the average composition of W:42.1, V:42.3, Cr:16.4, Mn:0.2 (table 15) which contains almost negligible amount of Mn and less amount of Cr compare with theoretically expected 25 atomic %, this is because of the high vapor pressure of Mn and Cr at high temperatures (note that vapor pressure of Mn is higher than Cr at any temperature).
- In arc melted WCrMnV HEA, composition of dendritic regions and inter-dendritic regions were found out to be W:61.9, V: 31, Cr: 6.6, Mn :0.5 and W: 12, Cr: 19.4, Mn:0.3, V:68.3 respectively (table 15). So, dendritic region was tungsten and Vanadium rich while inter-dendritic region was Vanadium and Chromium rich
- Arc melted WCrMnV HEA Shows single BCC phase with lattice constant of 3.1035 Å as shown in fig 17(a) and table 21 along with un-melted tungsten (fig 13(a))
- After levitation melting of above arc melted alloy with addition of Cr and Mn, we have found out equiatomic composition in grey region and composition of white was W: 62.4, V: 33.4, Cr: 3.5, Mn:0.7 as shown in fig 14(b) and table 16. This is because of diffusion of Mn and Cr (which were liquid in state during melting) in arc melted alloy. From fig 14(c) and table 17, we can infer that W and V from arc melted alloy (which remain solid or semi-solid during melting) diffuse towards outside region of MnCr binary alloy in less amount [20].
- we have tried to synthesized the HEA by powder route for comparative study. Ball milling was done for mechanical alloying followed by compaction (for conventional sintering) and then densification was done by conventional and spark plasma sintering

- Conventional and spark plasma sintered samples shows three different regions as shown in fig 15(a) ,16 and table 18,20 where region 1 is W,Cr and V rich, region 2 is W rich and region 3 is Mn,Cr,V and O rich
- 20 hours ball milled powder shows the single BCC phase formation with lattice constant of 3.1653 Å, as we can see from fig 17(b) and note that BCC phase formation is indicated by shift in peaks position and decrease in peak intensities of V and Cr
- In 20 hours, ball milled powder sample, we have seen peaks of Mn,Cr and V but their intensity was less and diminishing at higher 2 theta values
- XRD of both conventional and spark plasma sintered samples were index with BCC as a major phase with lattice constant of 3.1196 Å. But, Mn_{9.54}Cr_{14.40}O₃₂ (Cubic, Space group: Fd-3m (227), a=8.447 Å) was indexed as a minor phase present in conventional sintered sample while spark plasma sintered sample has some unknown phase(s) which is/are yet to be indexed.

5 CONCLUSION AND FUTURE SCOPE

Conclusion

In the present study, the structure and mechanical properties of the AlNbTiVZr HEA was examined and following conclusions were drawn.

1. Proper synthesis route for AlZrNbTiV HEA was established with the help Levitation Melting unit and conclusion was drawn that Levitation melting is better than Vacuum Arc Melting as it takes less time for melting and better homogeneity can be achieved by only one-time melting. In the as solidified condition, the AlNbTiVZr HEA was composed from B2(ordered BCC) phase in dendritic region and hexagonal ZrAl₂ and Zr₅Al₃ type phase particles in inter-dendritic region which was confirmed by using SEM, XRD and TEM techniques. The phase particles were enriched of Zr and Al while B2 phase was enriched of Nb,Ti and V. We can achieve single B2(ordered BCC) phase by controlling appropriate cooling rate of the sample.
2. After homogenization at 950 deg C for different times, we have not observed any drastic change in structural and mechanical properties. Then, we have homogenized the sample at 1200 deg C for 24 hours and observed recrystallized structure.
3. Homogenization of sample shows clustering of Zr and Al in one region (inter-dendritic for as cast and grain boundary for recrystallized structure) while rest of the elements form cluster in other region (dendritic for as cast and matrix for recrystallized structure)
4. Micro-hardness of the AlZrNbTiV HEA is directly proportional to fraction of second phase particles (ZrAl₂, Zr₅Al₃) which was deduced from the hardness values of homogenized samples [5]
5. AlZrNbTiV HEA has Single B2(ordered BCC) a major phase, low neutron absorption cross section, high hardness value and no major structural change at high temperature (900 deg c), hence, this alloy can be a potential candidate for fission based nuclear reactors e.g. fuel cladding material[4].

In the present study, WCrMnV HEA was synthesized (using melting route as well as powder route.) and characterized for the first time and following conclusions were drawn.

1. We have successfully synthesized the WCrMnV HEA (despite the evaporation problem of Mn and V) using Vacuum Arc Melting and Levitation Melting units. For comparative study and an attempt to find easy way for preparation, we have prepared this alloy using conventional and spark plasma sintering.

2. WCrMnV HEA prepared by melting route:
 - WCrMnV HEA Shows single BCC as a major phase (with lattice constant of 3.1035 Å) along with un-melted tungsten. Hence, it is must to find a way to solve un-melted tungsten problem.
 - WCrMnV HEA shows nearly equiatomic region and tungsten and vanadium rich region which can be explain by poor diffusivity of elements like Mn, Cr in tungsten.
3. WCrMnV HEA prepared by powder route:
 - Ball milled powdered for 20 hours shows single BCC phase but during sintering process powder gets oxidized (even though conventional sintering was done in Ar atmosphere and SPS was done in vacuum) and forms complex oxide phase containing Cr Mn, V and O. oxide was present in the alloys because of the oxidation of the powder of individual elements as they have more surface area exposed to environment.
 - WCrMnV HEA has 700 HV micro-hardness which shows that this alloy can possess better strength, hence this alloy has better strength, hardness, better corrosion resistance due to addition of Cr and low density of 10.52 g/cc which makes it a better candidate for plasma facing wall in fusion nuclear reactor.
4. WCrMnV HEA has BCC as a major phase, low density and high hardness value, hence, this alloy can be a potential candidate for plasma facing wall in fusion based reactors [15]

Future Scope

In present study we have only synthesized and characterized the two high entropy alloys, WCrMnV HEA for fusion based reactors and AlZrNbTiV HEA for fission-based reactors. But, their mechanical properties (like tensile strength, yield strength, creep strength etc) at room and high temperatures, phase stability at higher temperature (e.g. for fusion reactors, 550 deg C is working temperature), study of irradiation damage (e.g. Folded Tandem Ion Accelerator (FOTIA), BARC), Liquid metal corrosion behavior at higher temperature in Lead-lithium eutectic liquid for fusion reactor, Salt corrosion study for molten salt reactor (if AlZrNbTiV HEA shows required properties for molten salt reactors) etc. should be studied in future. WCrMnV HEA is difficult to synthesized (as Mn, Cr evaporates during melting and oxidation problem during ball milling). Hence, finding a way for this problem in future is a difficult and interesting task.

REFERENCES

- [1] Yvon, P., & Carré, F. (2009). Structural materials challenges for advanced reactor systems. *Journal of Nuclear Materials*, 385(2), 217–222.
- [2] XIA, S., WANG, Z., YANG, T., & ZHANG, Y. (2015). Irradiation Behavior in High Entropy Alloys. *Journal of Iron and Steel Research, International*, 22(10), 879–884.
- [3] Xian, X., Zhong, Z., Zhang, B., Song, K., Chen, C., Wang, S., ... Wu, Y. (2017). A high-entropy V 35 Ti 35 Fe 15 Cr 10 Zr 5 alloy with excellent high-temperature strength. *Materials & Design*, 121, 229–236.
- [4] Azevedo, C. R. F. (2011). Selection of fuel cladding material for nuclear fission reactors. *Engineering Failure Analysis*, 18(8), 1943–1962.
- [5] King, D. J. M., Cheung, S. T. Y., Humphry-Baker, S. A., Parkin, C., Couet, A., Cortie, M. B., ... Knowles, A. J. (2019). High temperature, low neutron cross-section high-entropy alloys in the Nb-Ti-V-Zr system. *Acta Materialia*.
- [6] Zinkle, S. J., & Busby, J. T. (2009). Structural materials for fission & fusion energy. *Materials Today*, 12(11), 12–19. doi:10.1016/s1369-7021(09)70294-9
- [7] Chen, W., Tang, Q. H., Wang, H., Xie, Y. C., Yan, X. H., & Dai, P. Q. (2018). Microstructure and mechanical properties of a novel refractory AlNbTiZr high-entropy alloy. *Materials Science and Technology*, 34(11), 1309–1315.
- [8] A. Kareer, J.C. Waite, B. Li, A. Couet, D.E.J. Armstrong, A.J. Wilkinson, Short communication: ‘Low activation, refractory, high entropy alloys for nuclear applications’, *Journal of Nuclear Materials* (2019).
- [9] O.N. Senkov, S.V. Senkova, C. Woodward, *Acta Mater.* 68 (2014) 214–228.
- [10] A. Takeuchi, A. Inoue, *Mater. Trans.* 46 (2005) 2817–2829.
- [11] INVESTIGATION OF HIGH-ENTROPY ALLOYS FOR USE IN ADVANCED NUCLEAR APPLICATIONS A thesis submitted in partial fulfilment for the degree of doctor of philosophy at University of Technology Sydney Daniel J. M. King
- [12] Chen, H.-L., Mao, H., & Chen, Q. (2018). Database development and Calphad calculations for high entropy alloys: Challenges, strategies, and tips. *Materials Chemistry and Physics*, 210, 279–290.
- [13] Durga, A., Hari Kumar, K. C., & Murty, B. S. (2012). Phase Formation in Equiatomic High Entropy Alloys: CALPHAD Approach and Experimental Studies. *Transactions of the Indian Institute of Metals*, 65(4), 375–380.

- [14] Gao, M. C., Carney, C. S., Doğan, Ö. N., Jablonksi, P. D., Hawk, J. A., & Alman, D. E. (2015). Design of Refractory High-Entropy Alloys. *JOM*, 67(11), 2653–2669.
- [15] Waseem, O. A., & Ryu, H. J. (2017). Powder Metallurgy Processing of a WxTaTiVCr High-Entropy Alloy and Its Derivative Alloys for Fusion Material Applications. *Scientific Reports*, 7(1).
- [16] Development of Induction Levitation Melter G. Sugilal, Shaji Karunakaran, Jyoti Jha, Shashi Kumar, M. H. Rao, C. P. Kaushik Nuclear Recycle Group
- [17] Khripunov, B. I., Koidan, V. S., Ryazanov, A. I., Gureev, V. M., Kornienko, S. . N., Latushkin, S. T., ... Zatekin, V. V. (2015). Study of Tungsten as a Plasma-facing Material for a Fusion Reactor. *Physics Procedia*, 71, 63–67.
- [18] Suri, A. K., Krishnamurthy, N. & Batra, I. S. Materials issues in fusion reactors. *J. Phys. Conf. Ser.* 208, 12001
- [19] Desecures, M. et al. Study of radioactive inventory generated from W-based components in ITER and PPCS fusion designs. *Fusion Eng. Des.* 88, 2674–2678,
- [20] Koch, F., Köppl, S. & Bolt, H. Self-passivating W-based alloys as plasma-facing material. *J. Nucl. Mater.* 386–388, 572–574.
- [21] Barron, P. J., Carruthers, A. W., Fellowes, J. W., Jones, N. G., Dawson, H., & Pickering, E. J. (2020). Towards V-based high-entropy alloys for nuclear fusion applications. *Scripta Materialia*, 176, 12–16.
- [22] Xian, X., Zhong, Z., Zhang, B., Song, K., Chen, C., Wang, S., ... Wu, Y. (2017). A high-entropy V 35 Ti 35 Fe 15 Cr 10 Zr 5 alloy with excellent high-temperature strength. *Materials & Design*, 121, 229–236.
- [23] <http://www.entall.imim.pl/calculator/>